




University of
Stavanger

FACULTY OF SCIENCE AND TECHNOLOGY

BACHELOR THESIS

Curriculum: Bachelor of Civil Engineering	Springsemester, 2021 Open
Author: Simen Riise	 (author signature)
Tutor: Gerhard Ersdal, Mostafa Ahmed Atteya	
Bachelor thesis title:	Experimental evaluation of the axial capacity of cracked tubular member
Credits (ECTS): 20	
Keywords: Buckling Columns Fatigue cracks Experiments NORSOK N-004 Strength	Number of pages: 57 + appendices/other: 17 Stavanger, 15/2021 date/year

Acknowledgments

Throughout the writing of this thesis, I have received a lot of support and assistance. I would first and foremost like to thank my supervisors Professor Gerhard Ersdal and Mostafa Ahmed Atteya, for the thesis suggestion and tremendous help and guidance throughout the entire project. Their expertise and passion have truly been inspiring and motivating.

I want to acknowledge Johannes Steinnes Jensen and Emil Surnevik Kristiansen for their great help in constructing the specimens and the crack simulation. I would also like to thank Jarle Berge and Samdar Kakay for their help with the test setup and the implementation of the tests. Finally, I would thank Magnus Våge for the Finite element model of the tests.

Summary

This thesis experimentally investigated the compressive axial capacity of cracked tubular members. Then compared it to NORSOK N-004 (Standard Norge 2004) formulae. Further, the test results were compared with other analytical models, such as non-linear finite element analysis from a separate thesis (Vågen 2021) and basic column formulae e.g. Perry Robertson and the Secant method.

In this study, 11 tubular columns were tested with a diameter of 70 mm, 2.9 mm thickness, and 1.5 m height, due to the testing facilities limitation. Different crack sizes were placed perpendicular to the loading direction with sizes corresponding to NORSOK N-004 reduced capacity of 25, 50 and 75%. The material properties were obtained by stub column tests. To further study the effect of cracks on tubular members, angled cracks with respect to the loading direction were introduced to the stub column.

For the specimens with cracks perpendicular to the loading direction, The test results were somewhat unexpected and showed an inconsiderable reduction in the axial capacity, as the crack surfaces bear on each other. However, the angled cracks introduced to the stub columns showed a considerable capacity reduction. The reduction is assumed to result from the crack surface slipping, discontinuity in the material, and torsion due to the angled crack in the stub column.

The conclusion was that angled cracks have the most significant impact on the compressive axial capacity. On the other hand, cracks placed perpendicular to the loading direction had an insignificant effect on the capacity. Hence, the NORSOK N-004 formulae provide inaccurate formulas for capacity determination for such cases. Among the analytical methods presented in this thesis, Perry Robertson gave the most accurate capacity. This result was somewhat expected as the method was best adapted to the actual column behavior in the tests.

Table of Contents

Acknowledgments	ii
Summary	iii
1 Introduction	1
1.1 Background	1
1.2 Problem statement	1
1.3 Overview of thesis	1
2 Buckling theory	2
2.1 Euler buckling	2
2.2 Column theory	3
2.3 Simplified column formulae	6
2.4 Material properties	8
2.5 Design code for capacity evaluation of steel columns	10
3 Test preparation and crack simulation	14
3.1 Introduction	14
3.2 Column test	14
3.3 Crack simulation	18
3.4 Test setup	22
3.5 Stub-column test	29
4 Test result	34
4.1 Introduction	34
4.2 Stub-column test	34
4.3 Column tests	35
4.4 Cracked stub-column test results	43
4.5 Discussion cracked stub-column test	45
4.6 Discussion of column test results	45
5 Comparison with analytical methods	49
5.1 Introduction	49
5.2 Comparison with empirical codified formulae	49
5.3 Comparison with non-linear finite element models	50
5.4 Comparison with analytical models	52
5.5 Discussion of comparison	54
6 Conclusion	55
7 References	56
Appendices	58
Appendix 1 – NORSOK N-004 Calculation	58
Appendix 2 – Perry Robertson and Secant Calculation	65

Table of Figures

Figure 1: Euler buckling curve illustrated (Osofero, 2021).....	3
Figure 2: second-order effect, load and lateral deflection. Described in webinar (AISC, 2005)	4
Figure 3: Local and global buckling, respectively (Mie.uth.gr, 2021)	5
Figure 4: Support conditions and corresponding k-factors (Ziemian R.D., 2010)	5
Figure 5: Euler buckling curve corrected by Johnson-Ostenfeld (Bai, Y. 2015)	8
Figure 6: Stress-strain curve showing the effect of strain aging and hardening from rapport (Britvec S. J., 1970)	9
Figure 7: Pipes 15	
Figure 8: Columns cutet from the pipes	16
Figure 9: Cutting the pipes	17
Figure 10: Milling the ends flat	17
Figure 11: Measuring and brushing of external steel	18
Figure 12: Change in natural axis due to crack. Moment due to eccentricity	19
Figure 13: Finding max lateral deflection y-max. Crack placement	20
Figure 14: Making the crack	21
Figure 15: Drilling holes and making filler material, respectively.....	21
Figure 16: Crack excluded and included filler	21
Figure 17: Test machin.....	22
Figure 18: Bottom plate, top plate and test setup used in (Vo T. & Hestholm K., 2019), respectively...	23
Figure 19: Technical drawing of the attachment cups by (Vo T. & Hestholm K., 2019)	23
Figure 20: Deformed bottom plate (Vo T. & Hestholm K., 2019).....	24
Figure 21: Impact on the stress strain curve due to the bottom plate deforming.....	24
Figure 22: Machining foundation and the final result, respectively.....	25
Figure 23: Bottom plate repair	25
Figure 24: Top and bottom support in test setup, respectively.....	26
Figure 25: DIC setup (Bmeafl, 2021) and speckle pattern used in the test, respectively	27
Figure 26: Geometric tolerances according to EN 10217-1 and measuring out of shape, respectively.	28
Figure 27: e.g. stress-strain curve from stub column test with material properties showed in (AISI, 2013)	29
Figure 28: Machining the endsurface plat.....	30
Figure 29: Attachment and cutting setup, respectively	31
Figure 30: Test setup requirements according to AISI S902-13	32
Figure 31: Test machine used for the stub column test	32
Figure 32: Stress strain curve, stub column test.....	34
Figure 33: Deformed shape stub columns.....	35
Figure 34: Max loading for test specimen.....	36
Figure 35: Load-displacement curve of each specimen	36
Figure 36: Photo of first five specimens.....	38
Figure 37: Deformed shape of cracked area (small, medium and large crack respectively).....	38
Figure 38: Load displacement curves for first five specimens.....	39
Figure 39: Photo of rotated specimens	40
Figure 40: Deformed shape of cracked area (small, medium and large crack respectively).....	41
Figure 41: Load displacement curves for rotated specimens	41
Figure 42: photo of specimens with larger holes.....	42
Figure 43: Deformed shape of cracked area (6, 8 and 10mm hole respectively)	42
Figure 44: Load displacement curves specimen with larger holes.....	43

Figure 45: Deformed shape stub columns	44
Figure 46: Stress strain curve stub column test	44
Figure 47: Normal condition local eccentricity and eccentricity due to holes and test setup, respectively	46
Figure 48: Rotated specimen identified as OD.....	47
Figure 49: Deformed shape column	48
Figure 50: Comparison – test result and NORSOK N-004 calculation.....	50
Figure 51: Comparison – test result and ABAQUS	51
Figure 52: Finite element model of buckled shape with k factor 0.5 and 1.0, respectively (Vågen 2021)	52
Figure 53: Comparison – test result and analytical models.....	53
Figure 54: Comparison of the different analytical methods	54

List of Tables

Table 1: Maximum load intact stub column.....	35
Table 2: Test results for first five specimen	37
Table 3: Test result rotated specimens	39
Table 4: Test result specimen with larger holes	42
Table 5: Stub column tests results	43
Table 6: Cracked stub column capacity and finite element calculation	45
Table 7: Values for tests and calculation according to NORSOK N-004.	49
Table 8: Ultimate capacities for experimental tests and finite element method from Vågen (2021).....	51
Table 9: Ultimate capacities for experimental tests and calculation according to Perry Robertson and secant formula.....	53

Appendices

Appendix 1 – NORSOK N-004 Calculation	58
Appendix 2 – Perry Robertson and Secant Calculation	65

1 Introduction

1.1 Background

As shown in (Ersdal, 2019), a significant part of the existing offshore facilities is now ageing. For these structures, after many years of undergoing substantial cyclic stresses, these structures will in many cases experience fatigue cracking, which in many cases requires repairs, decommissioning or rebuild. For this decision, knowledge about several issues are vital; one of them is how the capacity can be determined as a result of these ageing mechanism. Some experimental research has been done on corroded steel members, (Ostapenko A, 1999), (Hebor & Ricles, 1994), and at UiS also (Vo T. & Hestholm K., 2019). However, no experiments on the capacity of cracked steel members have been identified in this project. Hence, as many offshore structures and jackets are made of tubular members, experimental research addressing the capacity of cracked tubular members is needed, both for axial loading and for combined axial and bending loading. However, the experiments in this thesis is limited to axial compression capacity of columns.

The experimental results in this thesis are compared to calculated capacities according to NORSOK N-004, finite element analysis by Abaqus and other analytical methods. The 2004 revision of NORSOK N-004 (Standard Norge 2004) includes formulae for determining the capacity of a cracked tubular member. NORSOK N-004 will be the basis for which crack size chosen in this experiments.

1.2 Problem statement

Tubular members in offshore structures subjected to fatigue cracks will have a reduced capacity. In this context, it is essential to know how the crack affects the capacity to decide the danger associated with the damage and the urgency for repair.

The goal of this thesis is to get an understanding of how cracks affect the axial capacity of tubes with an experimental approach. Furthermore, compare the experimental results with the 2004 revision of NORSOK N-004 and other analytical models, such as finite element and basic column formulae.

Finally, the thesis is limited to only study the axial compression capacity of cracked tubular members and will not include any tension experiments.

1.3 Overview of thesis

Chapter 2 covers basic buckling theory, material properties of steel, generally used column formulae and NORSOK N-004 formulae for axial compression of damage tubular member. In Chapter 3, the test preparations, choice of specimen and crack simulation are presented. The chapter will also cover the test setup and procedure used in the experiments. The test results and discussion are to be found in Chapter 4 and the comparison with analytical models is presented in chapter 5. Finally the thesis will be concluded in chapter 6.

2 Buckling theory

2.1 Euler buckling

Column buckling is well known in engineering. The phenomena can be explained as the sudden lateral or side sway deflection of a long, slender member supporting a compressive load. Such members are called columns. As column buckling often is related to a sudden and dramatic failure of a structure, it needs special attention in the design.

The tendency for a column to buckle or remain stable under compressive loading depends on its ability to resist moment. Hence, to determine the critical load, the relation between the internal moment and the deflected shape can be used.

$$EI \frac{d^2v}{dx} = M$$

The Swiss mathematician Leonhard Euler initially solved this problem in 1757. The critical load is therefore often referred to as the Euler load. When the critical load is reached, the column is in the elastic regime and on the verge of becoming unstable. The smallest external impact will make the column unstable, and it buckles (Hibbeler, 2018) The Euler buckling curve is presented in Figure 1 based on the slenderness ratio discussed in Section 2.2.2.

Euler formula for buckling:
$$P_{cr} = N_E = \frac{\pi^2 EI}{(kL)^2}$$

Where:

- P_{cr} maximum axial load on the column just before it begins to buckle. This load must not cause the stress in the column to exceed the proportional limit
- E modulus of elasticity for the material
- L length of the column
- k buckling factor (factor for correcting the effective length of the column)
- I least moment of inertia for the column's cross-sectional area

For the Euler formula to be valid, the column and loading need to meet several conditions: (Hibbeler, 2018)

- The column needs to be ideal, which means:
 - material is homogenous and linear elastic
 - perfectly straight column with no imperfections
 - the cross-section is constant throughout the length
- The load is applied through the centroid of the cross-section
- The column needs to be considerably slender

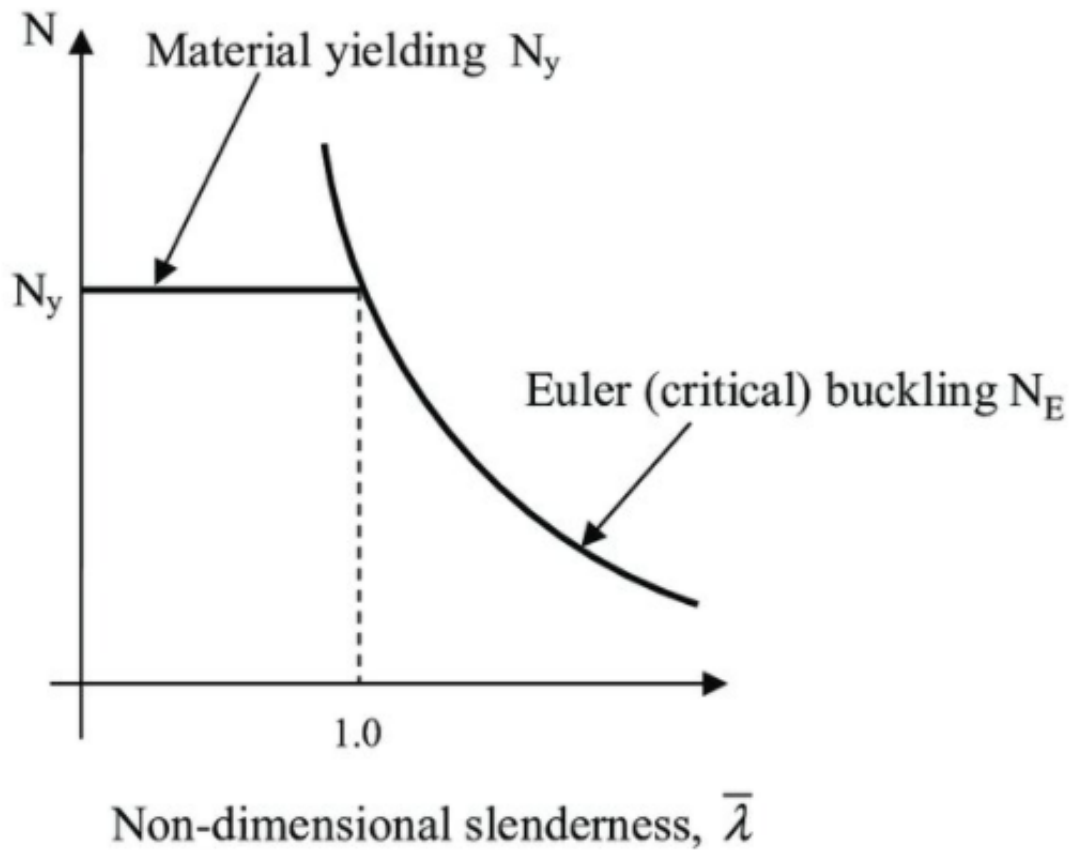


Figure 1: Euler buckling curve illustrated (Osofero, 2021)

2.2 Column theory

2.2.1 Imperfection

The Euler formula is the cornerstone for buckling theory. However, it only applies to idealized columns and loading. Alone it is not applicable for real columns. There will always be an eccentricity present from manufactory and the loading. In reality, the column never suddenly buckles; instead, they begin to bend ever so slightly immediately after the load is applied. This is known as the second-order effect shown in Figure 2. Further, another condition that's not meet in reality is the linear elastic behavior of the material. Many practical columns are in a range of slenderness, where the buckling portions of the column are no longer linearly elastic. This causes a reduction in stiffness and may result from non-linearity or partial yielding at a point on the cross-section with compressive residual stresses.

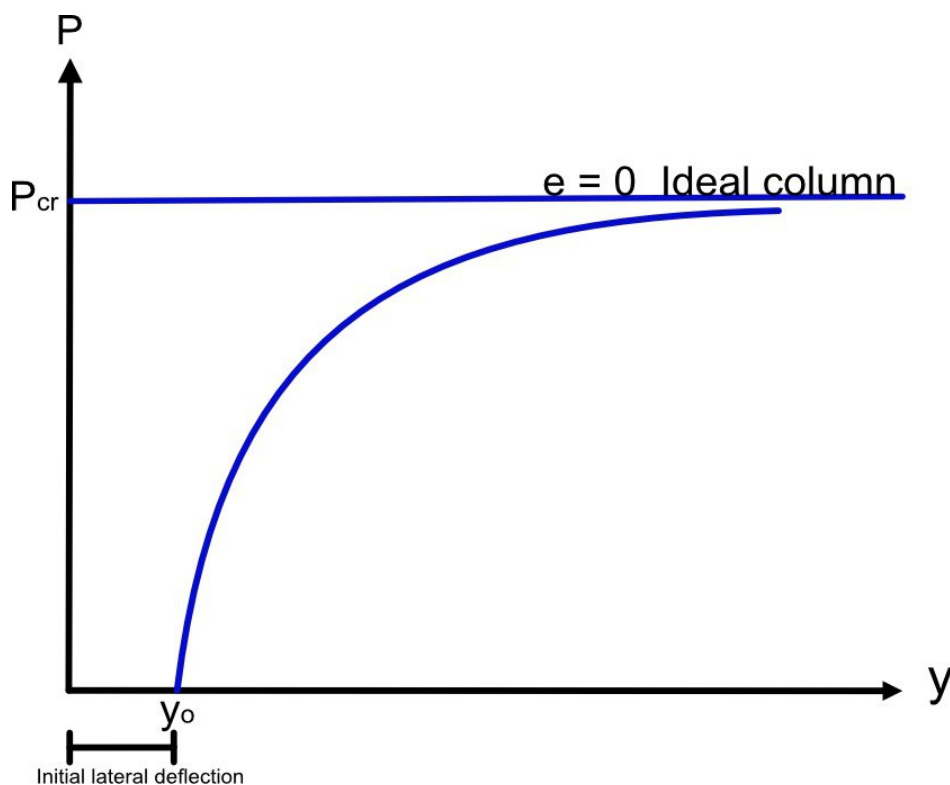


Figure 2: second-order effect, load and lateral deflection. Described in webinar (AISC, 2005)

For many columns, imperfection must be included to get a realistic maximum load. The column strength must be determined by including the imperfection, material non-linearity, and the effect of residual stresses. Hence, accurate determination of columns' maximum strength is a complicated process involving numerical integration, with the use of various solution procedures for non-linear problems.

2.2.2 Slenderness ratio

Within buckling theory, tubular steel columns are divided into three different categories based on their slenderness ratio. First are short columns, also called posts. These columns will not become unstable; instead, the material yields or fractures. Next is the intermediate columns, where stresses in parts of the cross-section become greater than the proportional limit, and the column fails due to inelastic buckling. The residual stresses present in the column and the imperfections in load and geometry play a prominent role in this type of failure. For these columns, the material strength will be the governing parameter, and the Euler load is inaccurate. The last category is the long and slender columns, where the moment capacity will be the governing parameter. These columns are subjected to elastic buckling and approaching the Euler load as the slenderness increase (Hibbeler, 2018).

2.2.3 Local buckling

Another important parameter for tubular columns is the diameter to thickness ratio. Columns with a large D/t ratio can be exposed to local buckling. In the design codes, the cross-section is classified based on the D/t ratio and the material strength. A combination of high material

strength and D/t ratio will put the column in a class where local buckling could be the failure mode (Ziemian, 2010). Damage columns can also be subjected to local buckling. To sum up, column buckling is controlled by the L/r ratio (slenderness), while local buckling dependent on the D/t ratio. These phenomena are shown in Figure 3.



Figure 3: Local and global buckling, respectively (Mic.uth.gr, 2021)

2.2.4 Effective length and support conditions

The axial capacity for a column is greatly dependent on the support condition. This was incorporated in the design code by introducing the well-known effective length factor k . This factor determines the effective length of the column based on the support conditions. Regarding the effect on column buckling, two restraints are of significant importance: Rotational fixed/free, translation fixed/free, and different combinations of these restraints. To obtain the effective length of a column, the k -factor is multiplied by the length. Figure 4 shows different support conditions and the respectively K -factor. As most theory, its idealized conditions, where the rotational and translation restraints are either complete or non-existence. Figure 4 also includes modified k values reflecting that neither perfectly fixity nor flexibility is attained in practice.

Buckled shape of column is shown by dashed line	(a)	(b)	(c)	(d)	(e)	(f)
Theoretical K value	0.5	0.7	1.0	1.0	2.0	2.0
Recommended K value when ideal conditions are approximated	0.65	0.80	1.2	1.0	2.10	2.0
End condition code						
		Rotation fixed, Translation fixed	Rotation free, Translation fixed	Rotation fixed, Translation free	Rotation free, Translation free	

Figure 4: Support conditions and corresponding k -factors (Ziemian R.D., 2010)

For design practice, simplified column formulae are provided, such as Perry Robertson and Johnson-Ostenfeld's corrections. These are empirical formulae. Hence, based on experiments and yield strength of columns.

2.3 Simplified column formulae

As the accurate determination of columns' maximum strength is a complicated process, several formulae are developed for capacity determination and design practice. Perry Robertson and Johnson-Ostenfeld's corrections are well-known empirical formulae based on experiments and yield strength of the column. Another procedure to determine the axial capacity is by not allowing the maximum stress to exceed the allowable stress or by a specific sideways/deflection of the column. The Secant formula is based on this method (Hibbeler, 2018).

2.3.1 Secant formula

Maximum deflection:
$$v_{max} = e \left[\sec \left(\sqrt{\frac{NL}{EI2}} \right) - 1 \right]$$

Maximum stress, secant formula
$$\sigma_{max} = \frac{P}{A} \left[1 + \frac{ec}{r^2} \sec \left(\frac{kL}{2r} \sqrt{\frac{N}{EA}} \right) \right]$$

Where:

- v_{max} maximum lateral deflection
- σ_{max} maximum elastic stress in the column (compressive stress)
- N vertical applied load to the column
- e eccentricity of the load P, measured from the centroidal axis of the column's cross-sectional area to the line of action of P
- c distance from the centroidal axis to the outer fiber of the column where the maximum compressive stress occurs
- A cross-sectional area of the column
- r radius of gyration

Both the maximum deflection and stress occur at the midpoint of the column $x = L/2$ for columns with identical boundary conditions (Hibbeler, 2018).

2.3.2 Perry Robertson equation

A widely used formula for defining the strength of a column is the Perry Robertson equation (1925). The equation is the background for buckling curves in a variety of design codes, such as Eurocodes.

The equation is derived on the assumption that imperfection could be allowed by giving the column an initial curvature. Further, the second-order effect is taken care of by adding an amplification term. The final derivation can be expressed as follows (Robertson, 1926):

$$\text{Robertson: } \sigma_u = \left[\frac{\sigma_y + (1+\eta)\sigma_e}{2} \right] - \sqrt{\left[\frac{\sigma_y + (1+\eta)\sigma_e}{2} \right]^2 - \sigma_y\sigma_e}$$

Where:

- σ_u the ultimate permissible applied stress
- σ_y yield stress
- σ_e Euler stress
- η imperfection variable
- w_0 initial deformation

The imperfection variable is refined based on experiments, which form the basis for the different buckling curves used in the Eurocode.

For beam-column with initial deflection and eccentric loading, the formula can be expressed: (Yong Bai, 2015)

$$\frac{N}{N_{ULT}} + \frac{N(w_0+e)}{M_{ULT}\left(1-\frac{N}{N_E}\right)} \leq 1.0$$

Where:

- N_{ULT} ultimate axial strength
- M_{ULT} ultimate moment capacity

2.3.3 Johnson – Osterfeld formula

Another known empirical formula is the Johnsons Osterfeld correction. Here the plasticity is accounted for by correcting the Euler buckling stress, as the buckling curve in Figure 5 shows. The equation is derived from column tests in the 1950th (Johnson 1966). The formula is used in several design codes and regulations, such as DNV (DNV GL, 2015).

$$\sigma_{ULT} = \sigma_E \quad \text{for } \frac{\sigma_E}{\sigma_y} \leq 0.5$$

$$\sigma_{ULT} = \sigma_y \left[1 - \frac{1}{4} \frac{\sigma_E}{\sigma_y} \right] \quad \text{for } \frac{\sigma_E}{\sigma_y} \geq 0.5$$

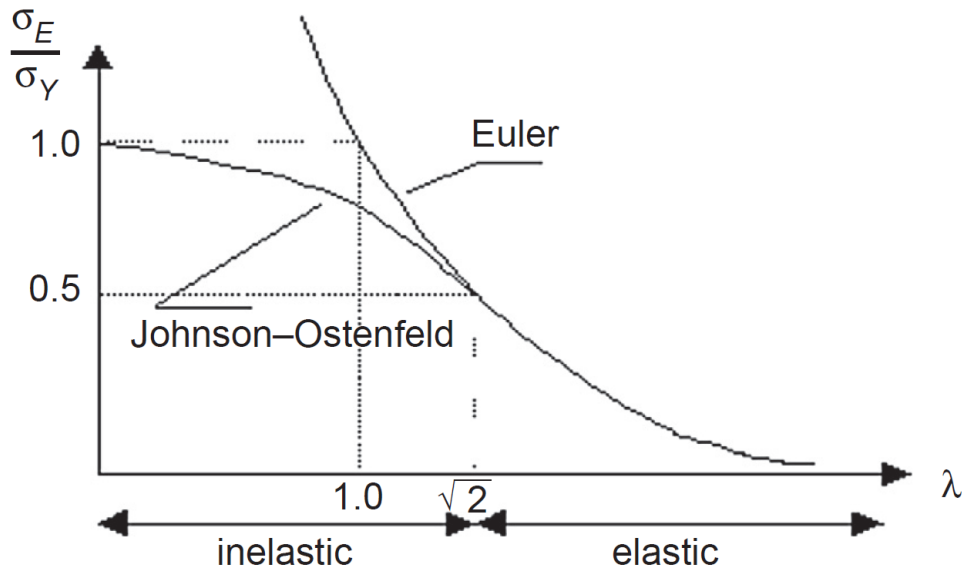


Figure 5: Euler buckling curve corrected by Johnson-Ostenfeld (Bai, Y. 2015)

2.4 Material properties

2.4.1 Carbon steel in general

Material strength and properties will have a significant impact on the behavior and strength of a column. Carbon steel is divided into different strength classes dependent on their yield strength, where the amount of carbon in the steel is the governing parameter. Higher steel grade has a larger amount of carbon, which gives the material higher strength. Furthermore, high carbon steel is more brittle than mild steel, which has lower strength and larger ductility. The ductility of a material describes the ability to deformed plastically before fracture. In many cases, ductile material is preferred as the failure is less sudden compared to a brittle material (Tubecon, 2021).

When loading steel, it will first behave elastic, meaning that it will go back to its original shape when unloaded. Further loading will make the material reach the plastic regime where stress-strain is no longer proportional, and the material will have permanent deformations. The stress-strain curve of compression or tension tests contains information describing the material properties. The following expression is essential material properties that can be obtained from the stress-strain curve:

Yield point: the maximum stress recorded in compression or tension test of steel before entering the plastic range.

Yield strength: the stress at which there is a specific deviation from an extension of the initial linear stress-strain plot, commonly taken as the intersection of the stress-strain curve and a lined 0.2% strain offset and parallel to the linear portion of the curve.

Ultimate strength: maximum stress recorded in tension or compression test

Young's modulus: the slope of stress-strain curve inelastic regime

2.4.2 Cold-formed steel tubes

Cold-formed steel is first rolled to the correct thickness then formed into tubes while the material is cold. Finally, the joint is welded. Hence, the material is subjected to plastic deformation, which results in strain hardening and strains aging of the material. This mechanism leads to an increase in the yield strength and reduction in ductility of the material, as shown in Figure 6.

Strain hardening: when a material is loaded beyond the yield point, the material will harden. Further, the material will follow the Young's modulus when unloaded. The point of max load will then be the new yield point.

Strain aging: If steel is plastically stretched and it takes a while before reloaded, a further increase in the yield strength occurs (Britvec S. J., 1970).

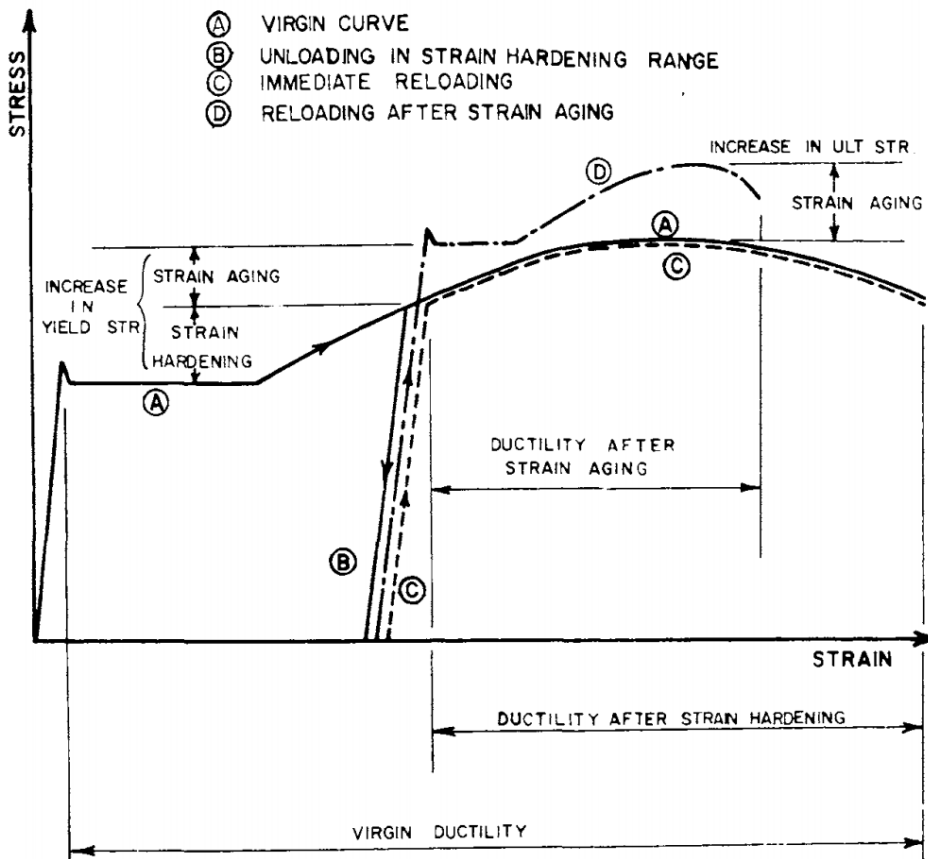


Figure 6: Stress-strain curve showing the effect of strain aging and hardening from rapport (Britvec S. J., 1970)

Cold-formed steel has a considerable amount of residual stresses present in the material due to the cold forming process. Thus, there will be a change in the stress-strain behavior from the basic material properties. Cold-formed tubes will exhibit a gradual yielding behavior and have a lower Young's modulus than hot-rolled steel (Ziemian R.D., 2010).

2.5 Design code for capacity evaluation of steel columns

For the design of tubular members in Norway, there are two commonly used standards. NS-EN 1993-1-1 design code for onshore structures and buildings design. This design code is based on Eurocode 3: Design of steel structures. For offshore structures, the Norwegian petroleum industry has developed a standard called NORSOK N-004, which is based on internationally recognized standards and additional provisions necessary to fill the needs of the Norwegian petroleum industry. As this thesis is aimed at offshore structures, NORSOK N-004 will be the standard presented and used in this thesis (Standard Norge 2004):

2.5.1 NORSOK N004 – Axial compression loaded column

Equation 6.3.3 in NORSOK N-004 provides a method for strength evaluation of tubular members subjected to axial compressive load:

Tubular members subjected to axial compressive loads should be designed to satisfy the following condition:

$$N_{Sd} \leq N_{c,Rd} = \frac{A f_c}{\gamma_M} \quad (6.2)$$

where:

N_{Sd} design axial force (compression positive)
 f_c characteristic axial compressive strength
 γ_M material factor

In the absence of hydrostatic pressure, the characteristic axial compressive strength for tubular members shall be the smaller of the in-plane or out-of-plane buckling strength determined from the following equations:

$$f_c = [1.0 - 0.28\bar{\lambda}^2]f_y \quad \text{for } \bar{\lambda} \leq 1.34 \quad (6.3)$$

$$f_c = \frac{0.9}{\bar{\lambda}} f_y \quad \text{for } \bar{\lambda} > 1.34 \quad (6.4)$$

$$\bar{\lambda} = \sqrt{\frac{f_{cl}}{f_E}} = \frac{kl}{\pi i} \sqrt{\frac{f_{cl}}{E}} \quad (6.5)$$

where:

f_{cl} characteristic local buckling strength
 $\bar{\lambda}$ column slenderness parameter
 f_E smaller Euler buckling strength in y or z direction
 E Young's modulus of elasticity, $2.1 \cdot 10^5$ MPa
 k effective length factor
 l longer unbraced length in y or z direction
 i radius of gyration

The characteristic local buckling strength should be determined from:

$$f_{cl} = f_y \quad \text{for } \frac{f_y}{f_{cle}} \leq 0.170 \quad (6.6)$$

$$f_{cl} = \left(1.047 - 0.274 \frac{f_y}{f_{cle}}\right) f_y \quad \text{for } 0.170 < \frac{f_y}{f_{cle}} \leq 1.911 \quad (6.7)$$

$$f_{cl} = f_{cle} \quad \text{for } \frac{f_y}{f_{cle}} > 1.911 \quad (6.8)$$

and

$$f_{cle} = 2C_e E \frac{t}{D}$$

where:

f_{cle}	characteristic elastic local buckling strength
C_e	critical elastic buckling coefficient = 0.3
D	outside Diameter
t	wall thickness

For $\frac{f_y}{f_{cle}} > 0.170$ the tubular is a class 4 cross-section and may behave as a shell. Shell structures may have a brittle structure failure mode. Reference is made to 6.2. For class 4 cross-sections, increased γ_M values shall be used according to Equation (6.22).

2.5.2 NORSOK N004 – Cracked column

The 2004 revision of NORSOK includes formulae for determining axial compression capacity of cracked tubular members subjected to pure compression or bending moment and compression combined (Standard Norge 2004):

Partially cracked tubular members equation 10.7.2

In lieu of refined analyses, partially cracked members with the cracked area loaded in compression can be treated in a similar manner to the one discussed for dented tubulars, see 10.6.2. An equivalent dent depth can be estimated from Equation (10.10), and the resulting resistance calculated from Equation (10.7).

$$\frac{\bar{\delta}}{D} = \frac{1}{2} \left(1 - \cos\left(\pi \frac{A_{Crack}}{A}\right)\right) \quad (10.10)$$

where:

$\bar{\delta}$	equivalent dent depth
D	tube diameter
A_{Crack}	crack area
A	full cross-section area

10.6.2.2 Axial compression

Dented tubular members subjected to axial compressive loads should be assessed to satisfy the following condition:

$$N_{sd} = N_{dent,c,Rd} = \frac{N_{dent,c}}{\gamma_M} \quad (10.2)$$

$$N_{dent,c} = \begin{cases} \left(1.0 - 0.28\bar{\lambda}_d^2\right) \xi_c \cdot f_y A_0 & , for \bar{\lambda}_d \leq 1.34 \\ \frac{0.9}{\bar{\lambda}_d} \xi_c f_y A_0 & , for \bar{\lambda}_d > 1.34 \end{cases} \quad (10.3)$$

where:

$N_{dent,c,Rd}$	design axial compressive capacity of the dented section	
$N_{dent,c}$	characteristic axial compressive capacity of dented member	
$\bar{\lambda}_d$	reduced slenderness of dented member, which may be calculated as	
	$\sqrt{\frac{N_{dent,c}}{N_{E,dent}}} = \sqrt{\frac{\xi_c}{\xi_M}} \cdot \bar{\lambda}_0$	
$\bar{\lambda}_0$	reduced slenderness of undamaged member	
ξ_c	$\exp\left(-0.08\frac{\delta}{t}\right)$ for $\frac{\delta}{t} < 10$	(10.4)
ξ_M	$\exp\left(-0.06\frac{\delta}{t}\right)$ for $\frac{\delta}{t} < 10$	
δ	dent depth	

The bending moment capacity can be determined from the following formula for cracked members subjected to bending moment.

10.6.2.3 Bending

Dented tubular members subjected to bending loads should be assessed to satisfy the following condition:

$$M_{Sd} \leq M_{dent,Rd} = \begin{cases} \xi_M M_{Sd} & \text{if the dented area acts in compression} \\ M_{Rd} & \text{otherwise} \end{cases}$$

where:

M_{Sd}	design bending moment
$M_{dent,Rd}$	design bending capacity of dented section
M_{Rd}	design bending capacity of undamaged sections, as given in 6.3.
	$\frac{f_m W}{\gamma_M}$
f_m	characteristic bending strength
W	elastic section modulus
Z	plastic section modulus

$$f_m = \frac{Z}{W} f_y \quad for \frac{f_y D}{Et} \leq 0.0517 \quad (6.10)$$

$$f_m = \left(1.13 - 2.58 \left(\frac{f_y D}{Et}\right)\right) \left(\frac{Z}{W}\right) f_y \quad 0.0517 < \frac{f_y D}{Et} \leq 0.1034 \quad (6.11)$$

$$f_m = \left(0.94 - 0.76 \left(\frac{f_y D}{Et}\right)\right) \left(\frac{Z}{W}\right) f_y \quad 0.1034 < \frac{f_y D}{Et} \leq 120 \frac{f_y}{E} \quad (6.12)$$

When exposed to crack, the combination of bending moment and axial compression the column experience needs to be combined when checking the capacity. The interaction formula provided in NOROK N-004 is based on the Perry Robertson formula presented earlier (Standard Norge 2004):

10.6.2.4 Combined loading

Dented tubular members under combined loading should be assessed to satisfy the following condition:

$$\frac{N_{Sd}}{N_{dent,c,Rd}} + \sqrt{\left(\frac{N_{Sd} \cdot \Delta y_2 \cdot C_{m1} \cdot M_{1,Sd}}{\left(1 - \frac{N_{Sd}}{N_{E,dent}}\right) M_{dent,Rd}}\right)^\alpha + \left(\frac{N_{Sd} \cdot \Delta y_1 \cdot C_{m2} \cdot M_{2,Sd}}{\left(1 - \frac{N_{Sd}}{N_E}\right) M_{Rd}}\right)^2} \leq 1.0 \quad (10.7)$$

$$\alpha = \begin{cases} 2 - 3 \frac{\delta}{D} & \text{if the dented area acts in compression} \\ 2 & \text{otherwise} \end{cases} \quad (10.8)$$

$M_{1,Sd}$	design bending moment about an axis parallel to the dent
$M_{2,Sd}$	design bending moment about an axis perpendicular to the dent
$N_{E,dent}$	Euler buckling strength of the dented section, for buckling in-line with the dent $\pi^2 \frac{EI_{dent}}{(kl)^2}$
I_{dent}	moment of inertia of the dented cross-section, which may be calculated as $\xi_M \cdot I$
I	moment of inertia of undamaged section
Δy_1	member out-of-straightness perpendicular to the dent
Δy_2	member out-of-straightness in-line with the dent
$C_{m1} C_{m2}$	moment reduction factor, as defined in Table 6-2

In the test, the columns are only subjected to axial compression. Any resulting moment is due to eccentricity due to the crack. Thus, the interaction formula could be written as follows by setting the moment reduction factor equal to 1.0 $M_{1,Sd} = N_{Sd} \cdot \Delta y_2$ simplified:

$$\frac{N_{Sd}}{N_{dent,c,Rd}} + \sqrt{\left(\frac{N_{Sd} \cdot \Delta y_2}{\left(1 - \frac{N_{Sd}}{N_{E,dent}}\right) M_{dent,Rd}}\right)^\alpha} \leq 1.0 \quad (10.7)$$

3 Test preparation and crack simulation

3.1 Introduction

This chapter will address the preparation of the test and specimen in addition to the crack simulation and assumptions. First, the column test will be presented, including the specimens chosen, crack simulation, assumption, and test setup and procedure. Finally, the stub column test procedure and specimen will be presented.

3.2 Column test

3.2.1 Overview

The test program consists of 11 columns with different cracks corresponding to a remaining capacity of 25%, 50%, and 75% of an Intact column according to the NORSOK standard. Furthermore, holes was drilled at the crack ends to replicate the repair method used for stopping cracks from progressing. Some samples were induced to different hole sizes to capture the stress concentration around the holes. To obtain the strain in the column, the crack, and around the holes, a DIC system was used. The test program also includes six stub-column tests, which was necessary to get the material properties.

3.2.2 Choice of specimen

When choosing specimens, there were several important considerations to take into account:

- Restriction in the test set up regarding geometry
- Maximum loading in the test setup
- Available material in the marked
- Pricing
- A good replicating of the members used in offshore structures

The machine used in the test was a bending moment machine configured for compression testing with a maximum loading capacity of 400 kN. For safety reasons, the loading capacity was lowered to about 50%. The test setup's attachments were made to only fit tubes with 70 mm diameter and a maximum height of 2 m. Further, the largest cross-sections possible within the machine's restraints were needed to replicate members used in the offshore structures, which led to choosing s235 steel, a relatively low grade.

The only pipe available meeting these restraints was cold-formed s235JRH 70,0 x 2,9mm x 6m, the same pipe used in corroded members' experiments by Vo et al (2019) at the University Of Stavanger. Unfortunately, these pipes were sold out. The tubes used in the test were P235TR1 made after EN 10217-1 with the same geometry. The difference between the two pipes is the steel grade. P235TR1 is designed to withstand high pressure and is suitable for transporting gas and fluid under moderately high pressure.

Since the pipe comes in lengths of 6 meters, the chosen length of the specimen was 1.5 m to get the most out of each pipe. The final specimen selected was as follow:

- Length: 1500 mm
- Diameter: 70 mm
- Thickness: 2.9 mm
- Type: Cold-formed P235TR1

These specimens have a D/t ratio of $24.2 < 50\epsilon$, which means class 1 cross-section, and a slenderness ratio of 63. Hence, the failure mode will be global inelastic buckling for the intact column. Such D/t and slenderness ratio is reasonably compared to tubular columns in offshore structures according to (Vo T. & Hestholm K., 2019).

The nominal yield strength for P235TR1 steel is 235 MPa. Usually, we can expect that the real value is about 20% higher than the nominal. Hence, it's cold-formed steel; the yield strength should be even higher due to strain hardening and aging caused by the plastic deformation in the cold forming process. A reasonable estimate for the yield strength will be obtained in the stub-column test. Using a yield of 280Mpa, the column should withstand a loading at around 200kN, which is about the maximum allowed loading in the test setup.



Figure 7: Pipes



Figure 8: Columns cut from the pipes

3.2.3 *Column preparation*

The pipes arrived in lengths of six meters as shown in Figure 7. Three pipes were ordered to be within the bachelor thesis budget, which gave 11 columns of 1.5 meters in height shown in Figure 8 and some material for the stub columns. First, all the columns were cut out in a band saw with cooling shown in Figure 9. Further, the ends were milled flat and perpendicular to the tube to be within the test procedure's requirements, as shown in Figure 10. A dial gauge was used to make sure the specimen was placed perpendicular to the milling tool. This also allowed checking the tube's initial out of straightness, which was ranging between 0.2 – 0.8 mm. Finally, the steel residues after the milling were removed using a metal brush shown in Figure 11. Ideally, the specimens should be cut out from a straight portion of the pipe to minimize the initial out of straightness. However, it is costly, and the pipes seem to have approximately the same out of straightness over the entire length.



Figure 9: Cutting the pipes



Figure 10: Milling the ends flat



Figure 11: Measuring and brushing of external steel

3.3 Crack simulation

3.3.1 Determine crack size

The crack sizes chosen were 12%, 23.5%, and 38.5% of the circumference. These crack sizes correspond to a respectively capacity reduction of 25%, 50%, and 75% of an intact column according to NORSOK N-004. In the calculation, it was assumed that the crack surface would be slipping under loading. Thus there will be non-considerable bearing on the cracks surfaces, which leads to a shift in the center of gravity in the damaged cross-section as shown in Figure 13. The shift is caused by the removed material from the holes and the slipping effect on the crack. As a result, an additional local moment will be present in the column because of the eccentricity in the damaged cross-section shown in Figure 12.

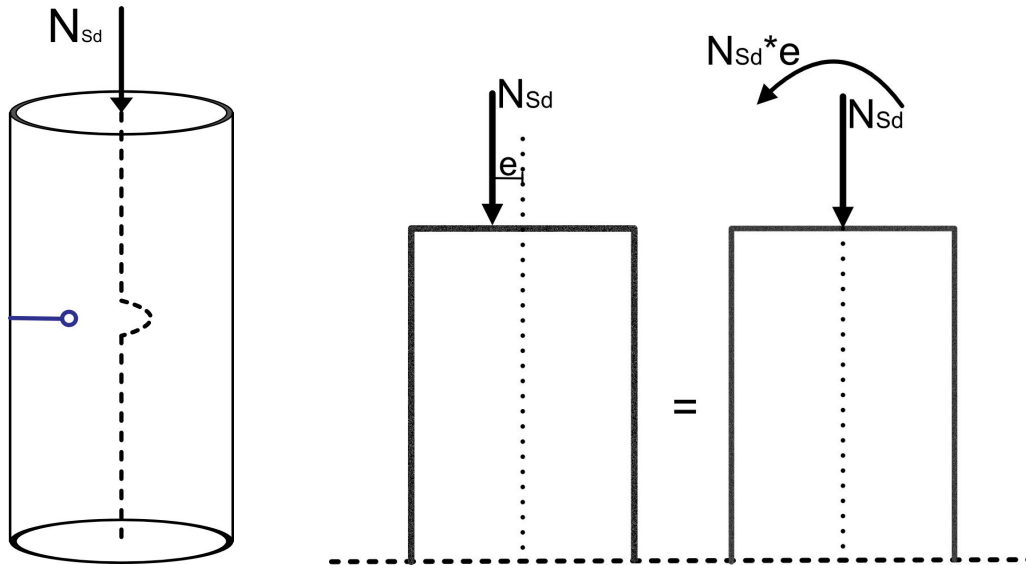


Figure 12: Change in natural axis due to crack. Moment due to eccentricity

Based on these assumptions the calculation procedure for cracked tubular member was as follow according to Norsok N-004:

- Use basic static theory to find the eccentricity in the cracked cross-section
- Use the Norsok formula to determine the equivalent dent depth
- Calculate the capacity of axially loaded dent tubular members according to Norsok N-004.
- Satisfy the interaction equation in Norsok N-004 for combined loading (bending and compression).

3.3.2 Crack placement

A parameter that's not considered in the Norsok standard is the placement of the crack. To obtain the maximum capacity reduction due to a crack, it needs to be placed where the maximum stresses occur. For ideal support conditions, this is relatively straightforward. For the test setup used in this experiment, there are many uncertainties related to the support condition, explained in more detail in Section 3.4.4. The method used to find the placement for the crack was as follows. First, an intact column was tested until failure. Then a straight edge was used to locate the point with the maximum lateral deflection on the column, which then became the basis for the crack placement as shown in Figure 13. It was also decided to put the crack parallel with the end surface of the tube to obtain the largest capacity reduction.

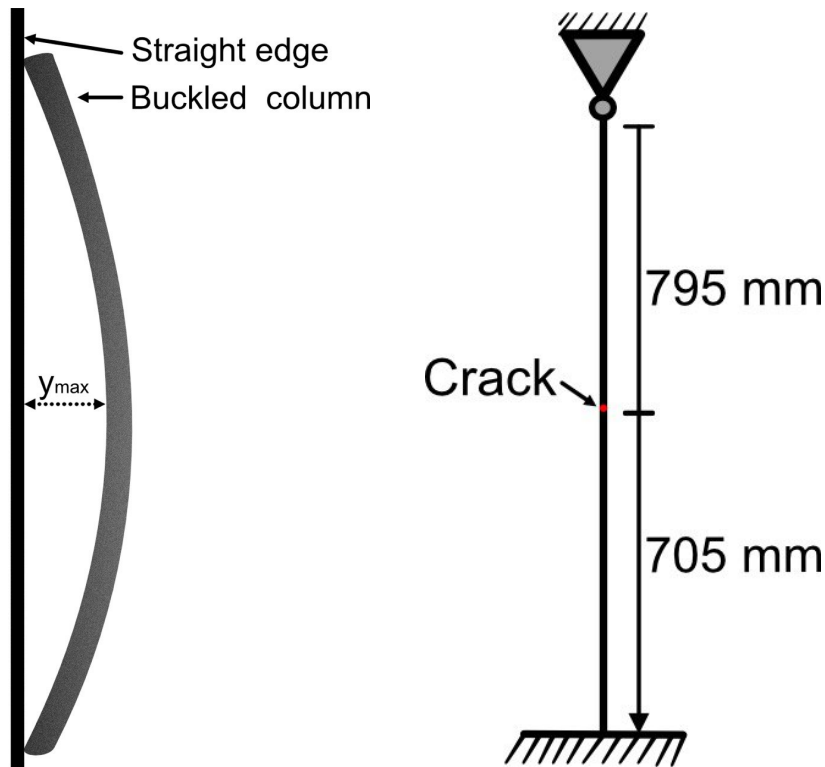


Figure 13: Finding max lateral deflection y_{\max} . Crack placement

3.3.3 Crack preparation

The specimens were put in a lathe, and an air-powered multi-cutter was attached to the tool holder. This way, it was possible to get thin and precise cuts shown in Figure 14. Further, cooling liquid was used to minimize the heat while cutting, as heat may change the material's residual stresses. Furthermore, the cut was filed to get an even cut thickness. Additionally, a filler material of the same pipe steel type was made in the lathe and placed in the cut to better replicate an actual crack's thickness. Finally, it was drilled holes in the crack ends. The filler and drilling of the holes is shown in Figure 15 and the final crack excluded and included filler is shown in Figure 16.

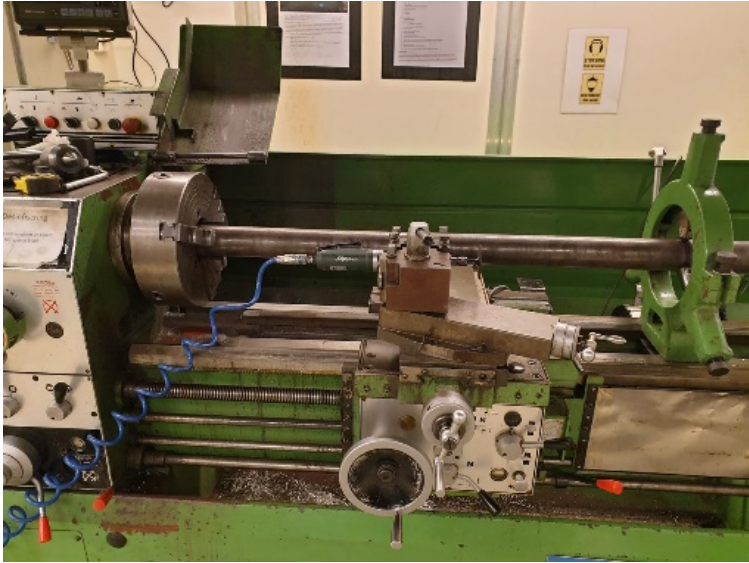


Figure 14: Making the crack



Figure 15: Drilling holes and making filler material, respectively

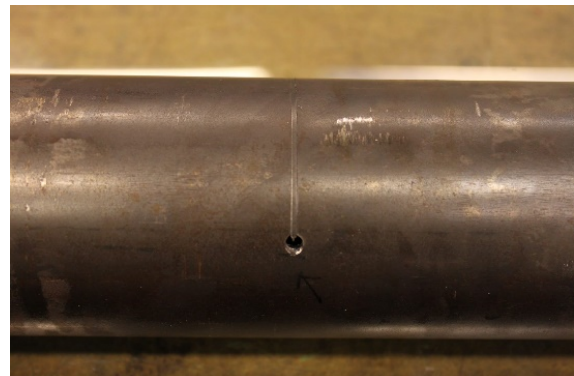


Figure 16: Crack excluded and included filler

3.3.4 Specimen notation

To be able to distinguish the specimens from each other, they were identified as follows:

Tube diameter – thickness – diameter hole size - the extent of damage as a percentage of the circumference - chronological test number within its group

For example, specimen 70-29-4-88-3 has a diameter of 70 mm, a thickness of 2,9 mm, hole size diameter of 4 mm, 88 % undamaged circumference (equivalent with a crack of 12%), and number 3 of its kind.

Some of the specimens have an additional OD in the identification, an abbreviation for "Opposite Direction." This describes the placement of the crack about the hinge mechanism. Ideally, turning the crack facing 180 deg should not influence the test result unless there is an eccentricity in the test setup.

3.4 Test setup

3.4.1 Test machine

The machine used in the test is a *TONI TECHNIK Baustoffprüfsysteme GmbH D-1000* Shown in Figure 17. This machine is intended for inducing bending moment to beams with a loading capacity of 400 kN. Hence, the test machine needed to be configured for compression testing of columns.

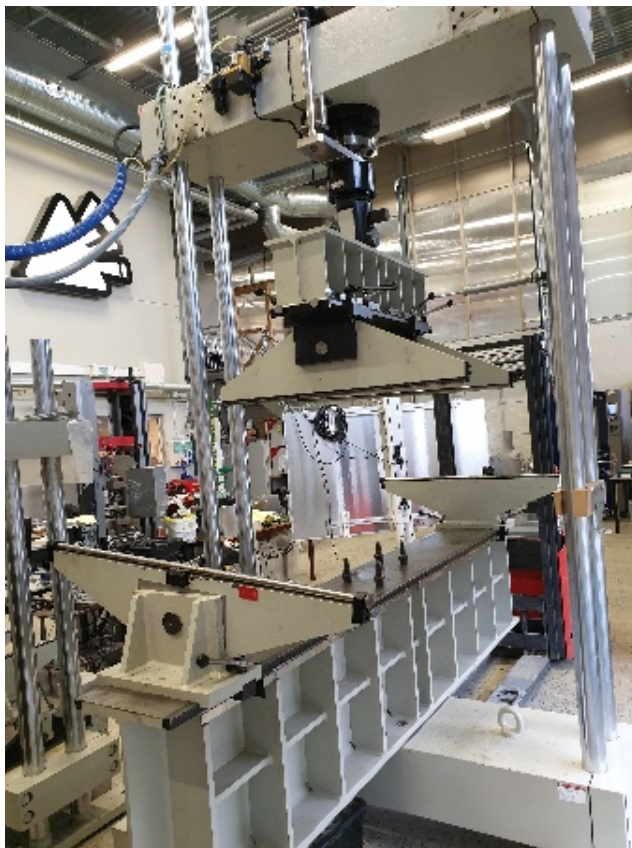


Figure 17: Test machin

The TONI TECHNIK has been used for compression testing of similar tubes with corrosion damage. Therefore the top and bottom attachments were already made, as shown in Figure 18. The attachment cups used was the ones made by Vo et al (2019) and the technical drawing is shown in Figure 20.



Figure 18: Bottom plate, top plate and test setup used in (Vo T. & Hestholm K., 2019), respectively

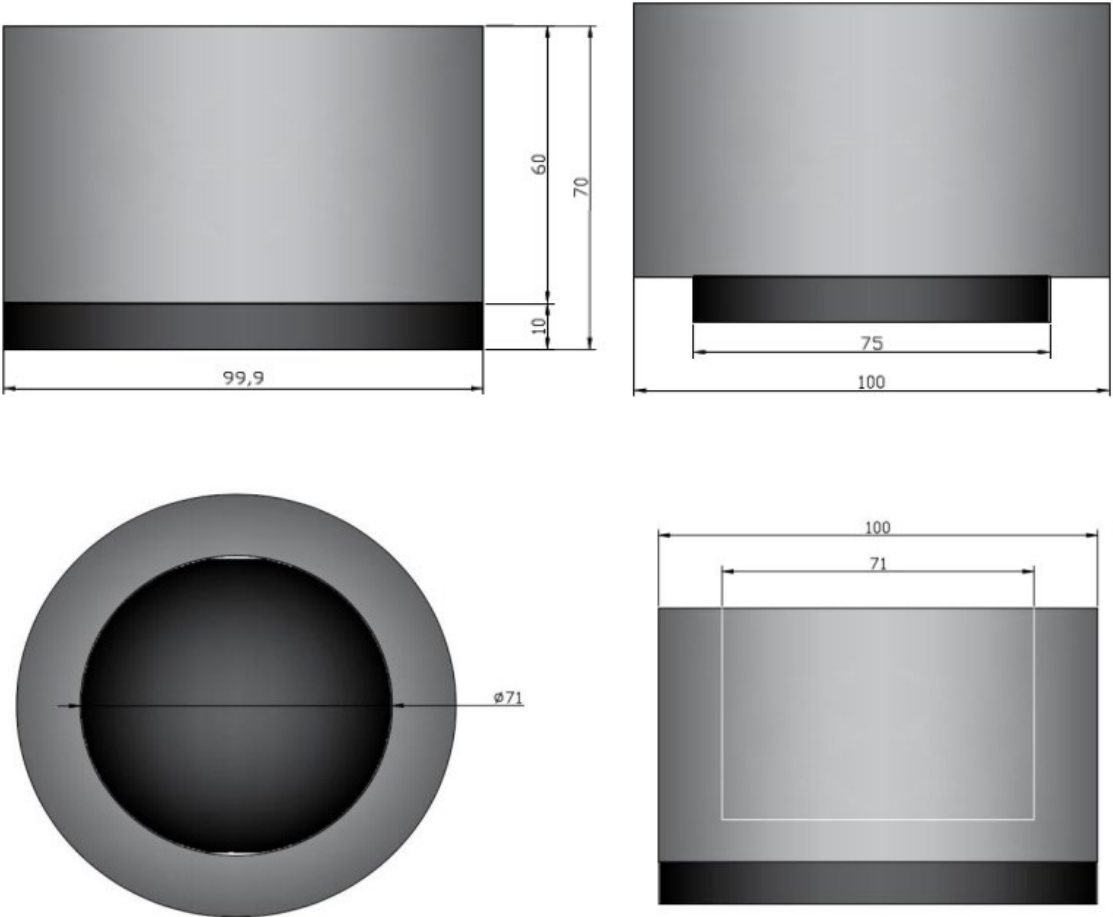


Figure 19: Technical drawing of the attachment cups by (Vo T. & Hestholm K., 2019)

3.4.2 Test setup improvement

The result from earlier testing shows that the test setup needs some improvements. When the column is buckling, the cup and bottom plate acting as fixed support experience a bending moment, which causes the plate to deform. Hence, the next test stress/strain curve will be damaged as the plate bend back in its original position. The damaged plate is shown in Figure 20 and the impact on the stress strain curve is shown in Figure 21.

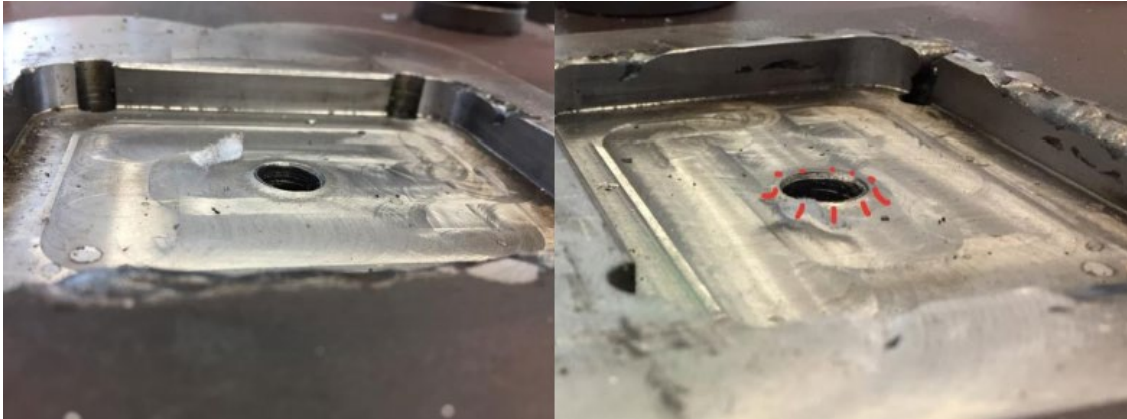


Figure 20: Deformed bottom plate (Vo T. & Hestholm K., 2019)

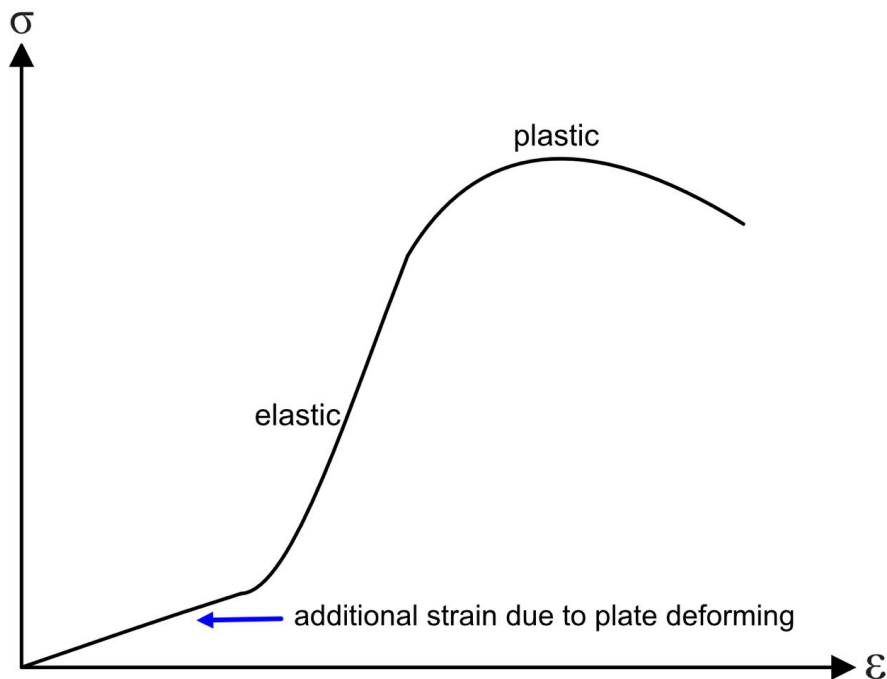


Figure 21: Impact on the stress strain curve due to the bottom plate deforming.

Furthermore, the distance between top and bottom was too large to fit the pipes. Usually, the loading head can be moved, but as this is a time-consuming process, it was decided to lift the bottom instead by making a foundation.

A massive stainless steel cylinder 150 mm in diameter was used as a foundation for the bottom attachment. Both ends and sides of the cylinder were machined in a lathe to get flat and parallel

surfaces. Next, it was drilled and threaded hole in the cylinder to strengthen the bottom attachment. Additionally, a stainless steel pipe was cut and machined in the lathe for bolt support, machining processes and result is shown in Figure 23. The reason for using stainless steel was that this was the best suitable residual material in the workshop. Stainless steel has a lower youngs modulus than carbon steel, which is unfortunate in a compression test. However, cold-formed steel tubes contain more residual stresses than hot-rolled, hence expecting a lower young modulus. Considering this and the cylinder is massive, the effect on the test result will be inconsiderable. Finally, the bottom plate was repaired in a milling cutter shown in Figure 23.

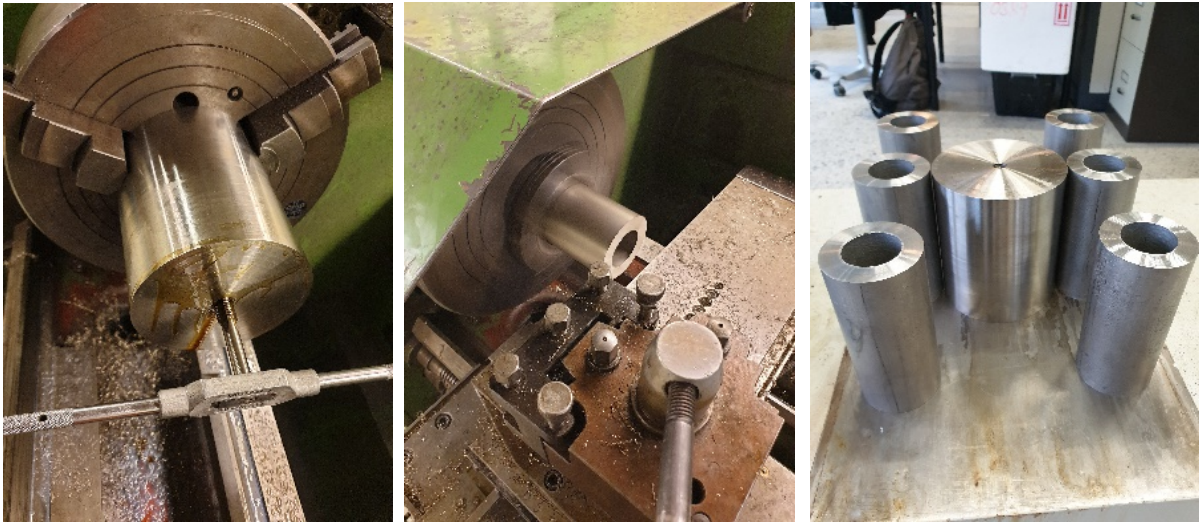


Figure 22: Machining foundation and the final result, respectively



Figure 23: Bottom plate repair

Another improvement that was wished to do was fixing the top attachment to remove some uncertainties regarding the hinge mechanism. The problem with this was that the loading cylinder would take a bending moment, possibly damaging the machine. Hence, it was decided to keep the hinge.

3.4.3 test setup

The supports of the test setup are fixed–pinned, where the bottom support fixed and the top one pinned. A detailed overview of the setup is shown in Figure 24.

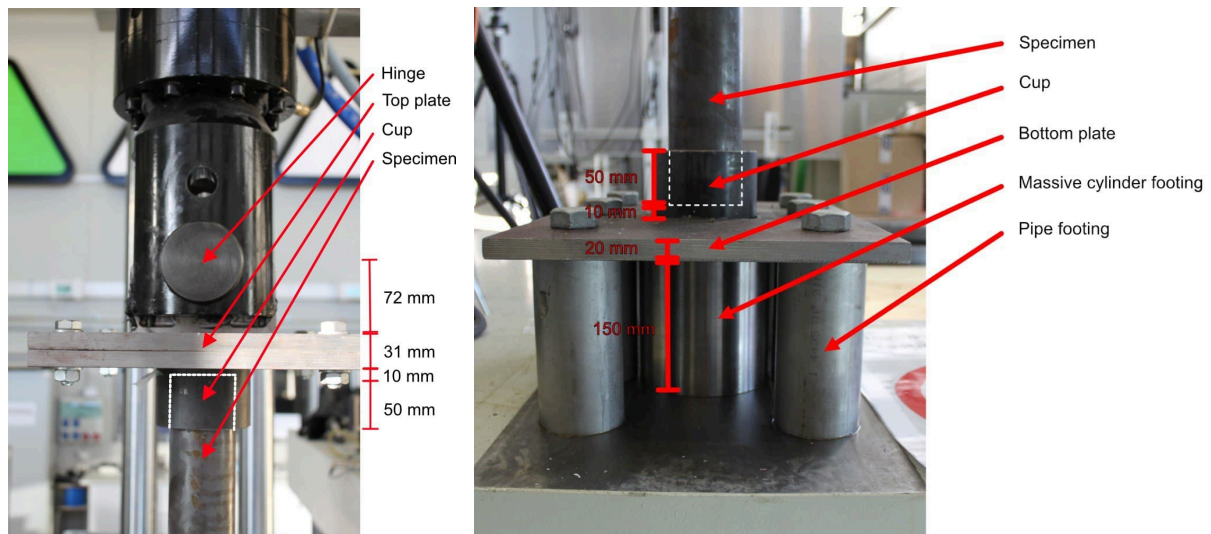


Figure 24: Top and bottom support in test setup, respectively

3.4.4 Test setup assumptions

The following assumptions have been made during testing:

- The pipe ends are flat and perpendicular to the load direction and have uniform pressure.
- The load is acting parallel and in the center of the tube.
- Any misalignment will cause additional moments due to eccentricity.
- The effects of end cups settlements on the specimen response are ignored.

Due to time and cost limitation, the supports were not welded and hence end fixation was not achieved. The effective column length is considered equal to the pipe length, while it may be reduced with the end cups length in reality. Further, Since circular hollow section stiffness is equally distributed around the neutral axis, the hinges should be spherical to allow the tube to buckle in any direction. Furthermore, the rotation point of the hinge should be placed at the column end. In the test setup, rotation was allowed only around one axis and the rotation point is moved 80 mm above the column end, possibly increasing the buckling length.

3.4.5 Digital image correlation (DIC) system

As shown in Figure 25, a DIC system was used during testing to map column response (strain and hence stress). The system is intended to provide information about local deformation and critical stress areas on the column, such as the crack and the holes. The DIC result can also be compared to the result from the test machine for validation.

The concept of DIC is to compare two images of the specimen before and after deformation. The strains and displacement are then determined by correlating the position of pixel subsets or blocks in the original and deformed image. A contrast speckle pattern is typically sprayed on

the surface to get better results. For the system to capture deformation in all directions in space, it uses two cameras calibrated to know their position in relation to each other (Lavigation, 2021).

The specimen in the test needed some preparations as the steel surface is smooth and of low contrast. The surface was first sprayed with white color, then a black speckle pattern, as shown in Figure 25. To be sure the paint sticks to the specimen under deformation, the surface was carefully sanded and cleaned with alcohol.

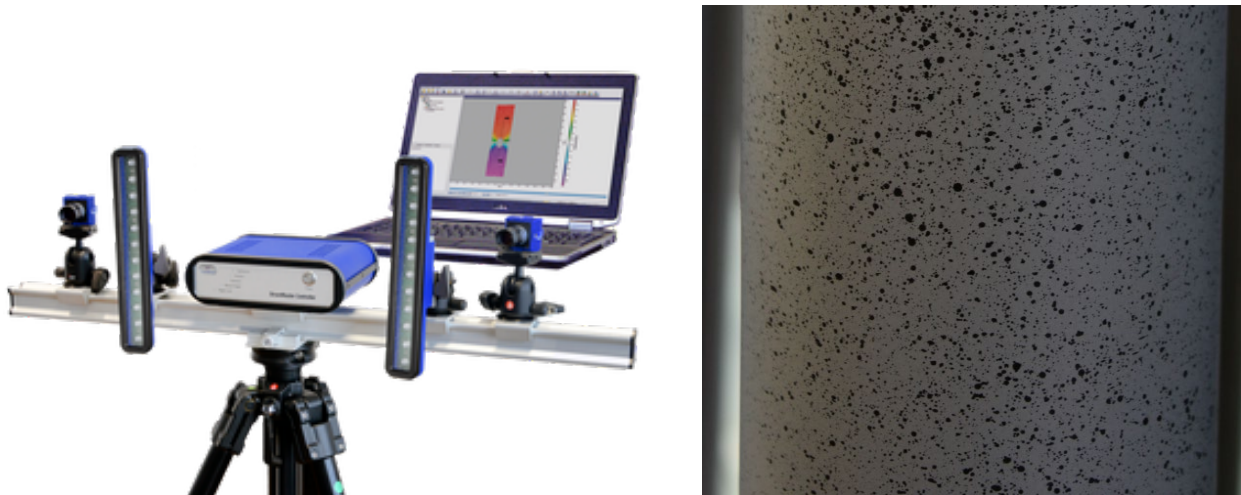


Figure 25: DIC setup (Bmeafl, 2021) and speckle pattern used in the test, respectively

3.4.6 Test Procedure

The test procedure used for the centrally loaded column test is according to Task Group 6 of the Column Research Council based on Lehigh University (Zieman, 2010), as described in appendix B.

Initial Measurements

The variation in the cross-sectional shape, area and initial out-of-straightness will affect the column strength. Hence, the initial dimensional measurements, including out-of-straightness, are an important step of the testing. The column thickness and diameter were measured with calipers. Furthermore, the out-of-straightness was measured by slowly spinning the specimen in a lathe and clocking the differences, as shown in Figure 27. Finally, the out of straightness was measured in the milling cutter by attaching a gauge clock to the machine and moving the specimen along the clock. Only some of the specimens were measured, all the imperfections were well below EN 10217-1 recommendation. In addition, the tubes were produced after EN 10217-1, which is relatively stringent regarding geometric characteristics, as shown in Figure 26.

Table 7 — Tolerances on outside diameter and wall thickness

Outside diameter <i>D</i>	Manufacturing process	Tolerance on outside diameter	Tolerance on wall thickness ^a		
			<i>T</i> ≤ 5	5 < <i>T</i> ≤ 10	10 < <i>T</i> ≤ 40
			≤ 219,1	EW and HFW	±1 % or ± 0,5 whichever is the greater
> 219,1	EW and HFW	±0,75 % or ± 6 whichever is the smaller	±8 % or ± 2 whichever is the smaller		
ALL	SAW	±0,75 % or ± 6 whichever is the smaller	±10 % or ± 0,3 whichever is the greater		±8 % or ± 2 whichever is the smaller

^a The plus tolerance excludes the weld area (see 8.7.4.2).

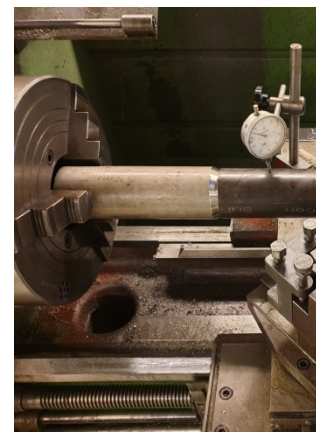


Figure 26: Geometric tolerances according to EN 10217-1 and measuring out of shape, respectively

Alignment

There are basically two methods for alignment with the test machine, which is an important step before testing. In the first method, the column is aligned under loading, such that the axial stresses are uniform over the cross-section at certain points. The second method is careful geometric alignment, which is the method used in this test. The second, geometrical alignment, is the recommended method as this is simple and time-saving.

Instrumentation

For these tests, the most important information is the ultimate strength of the column. Hence, the load and overall shortening of the column will be recorded by the test machine. Additionally, a DIC system will be used to give information about the strain. Other relevant information, such as lateral displacement, will not be recorded in this test program.

Test settings

The test should be started with an initial load of 1/15 to 1/20 of the estimated ultimate load capacity to preserve alignment establishment. Hence, the preload was set to 10 kN. Unfortunately, the preload setting changed to 5 kN (predefined settings) when the test started. As a result, it was decided to use the same preload on all tests to have a good basis for comparison.

Furthermore, the test loading rate was set to 4.2 kN/min, corresponding to about 6.9 MPa/min, which is the maximum loading rate recommended according to the procedure (Zieman, 2010). The loading rate is an essential parameter in distinguishing between ultimate static and dynamic load capacity and since this is a test of static load capacity, a low loading rate is used.

Testing

First, the specimens were placed in the test machine with the crack facing in the same direction as the hinge. Thus, induce the largest stresses on the damage. Further, to ensure that the test setup was working correctly, a specimen was loaded until 30% of the estimated yield strength. Young's modulus of the stress-strain curve was then compared to a rough estimate of young's modulus in the stub column test and former column test of corroded members. The result of the comparison showed an apparent similarity, and the test was ready to start.

The first specimen tested was an intact column used as a reference and basis for the crack placement. The point with the largest lateral deflection was measured and used for placing the crack. Next, it was tested four tubes with three different crack sizes, all with the crack facing the same direction. The specimen with the smallest crack (identified UP) was placed upside down in the test machine and had to be done again. Further, three specimens with the different crack sizes were tested with the crack facing the opposite direction (identified OD). Finally, the last three specimens with the medium crack size and different hole sizes were tested.

3.5 Stub-column test

3.5.1 Overview

Stub column tests were carried out to obtain the actual material properties. The reason for performing stub column tests instead of tension tests is because the cracked columns are tested in compression. Hence, the material properties in compression are needed. Furthermore, a tension test will give an inaccurate result because of the unevenly distributed residual stresses present in both tension and compression in the cold-formed tubes.

The procedure used in this test is the American standard (AISI, 2013). In addition to presenting the stress-strain curve, several data can be obtained from the tests:

- Youngs modulus of elasticity
- proportional limit stress,
- elastic, elastic-plastic, and plastic range,
- yield strength,
- yield stress level,
- onset of strain hardening,
- strain hardening range and
- strain hardening modulus,

An example of stress-strain curve from a stub column test is shown in Figure 27. For this thesis, however, the test target is to obtain the yield strength and youngs modulus of elasticity.

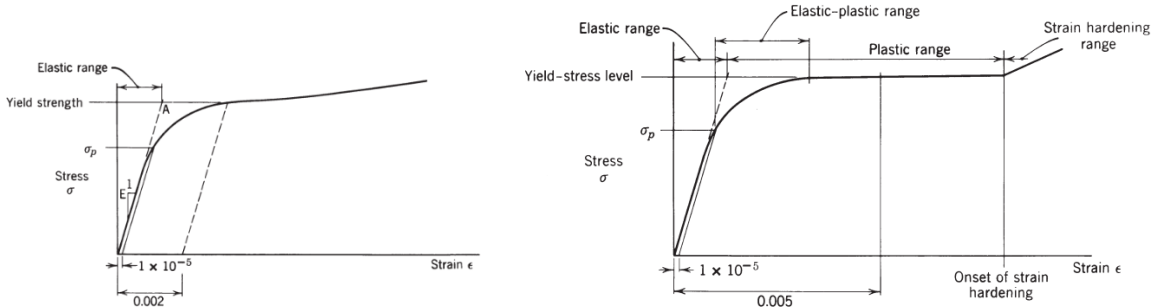


Figure 27: e.g. stress-strain curve from stub column test with material properties showed in (AISI, 2013)

The test consists of 6 stub column compression tests. Two intact specimens were tested to obtain the material properties, and the remaining four specimens were induced with the medium crack size and 4mm holes. However, three of the specimens had the crack rotated 45 and 90 degrees relative to the end surface.

3.5.2 Preparation of specimen

Procedure requirements

The specimens need to meet several requirements for obtaining reliable results from the stub column test:

- The length requirement shall be as follows:
 1. Length should not exceed 20 times the radius of gyration to eliminate the overall column buckling effect.
 2. Length should not be less than three times the greatest overall cross-section width to minimize the end effect under loading.
- The specimen's end surface should be cut to a flatness tolerance of plus or minus 0.0508 mm.
- The specimen should be cold sawed at a distance at least equal to the cross-section width from the pipe ends.
- The test should include at least three identical stub column specimens.

Stub column specimen preparation

The length chosen for the stub column was 234 mm, as this meets the standard requirements and the test machine capacity. The specimens were cut out 70 mm from the pipe ends with the same band saw used for the column specimens. Further, the ends were machined in a lathe to meet the end surface flatness requirements shown in Figure 28. Finally, the external steel was removed with a metal brush as for the column specimens.

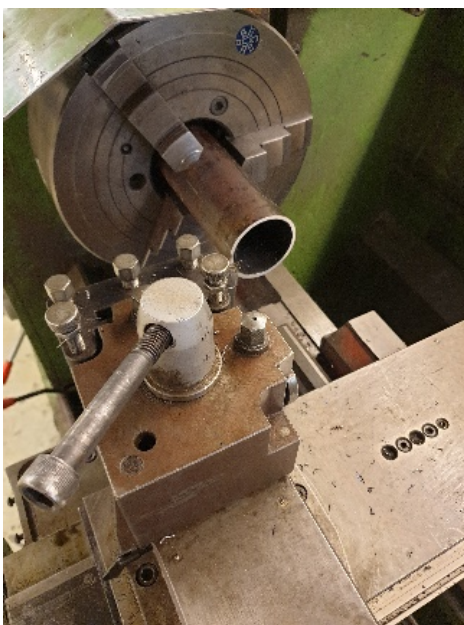


Figure 28: Machining the endsurface plat

Crack preparation

Four of the specimens were prepared with the medium crack size with 4 mm holes, of which one had the crack parallel to the end surface, two had the crack 45 degrees relative to the end surface, and one had the crack perpendicular to the end surface. The crack was placed in the center of the length of the specimen.

The crack was made the same way as for the column specimens. A pipe was machined as an attachment to fit the stub column specimens in the cutting setup, as shown in Figure 29.

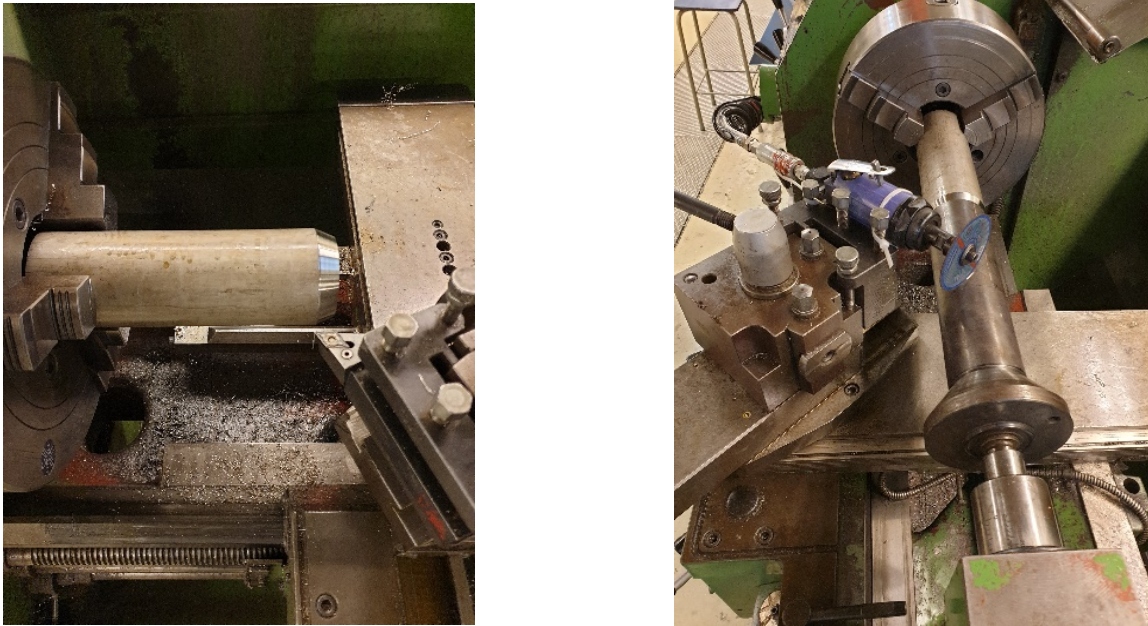


Figure 29: Attachment and cutting setup, respectively

Specimens notation

The specimens are identified the same way as the columns, but with an additional marking for the crack placement relative to the end surface.

Tube diameter – thickness – diameter hole size - the extent of damage as a percentage of the circumference – angel on crack relative to end surface - chronological test number within its group

As an example, specimen 70-29-4-76.5-45-2 has a diameter of 70 mm, a thickness of 2.9 mm, hole size diameter of 4 mm, 76.5 % undamaged circumference (equivalent with a crack of 23.5%), the crack is rotated 45 degrees relative to the end surface, and number 3 of its kind.

3.5.3 Setup and testing

Test machine

The machine used for the stub column compression test is a TONI-TECH 3000 kN compression machine shown in Figure 31. According to the standard, steel endplates should be used to transfer the load, and a layer of grout should be placed between the steel plate and the testing machine to facilitate aligning of the test specimen shown in Figure 30. As the test machine has a spherical bearing head, the grout layer wasn't needed.

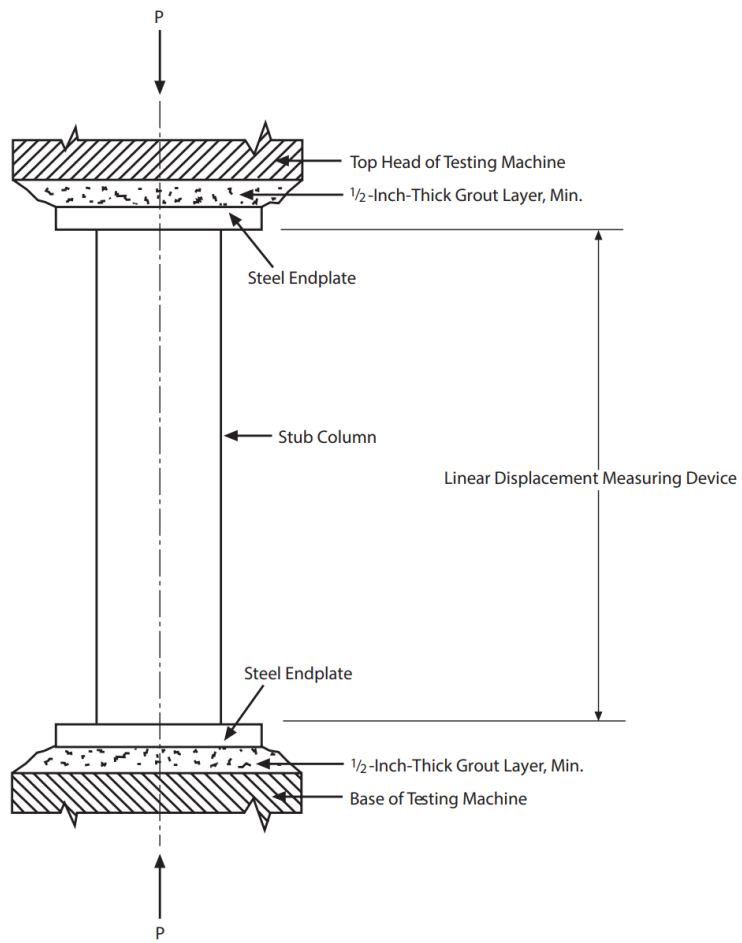


Figure 30: Test setup requirements according to AISI S902-13

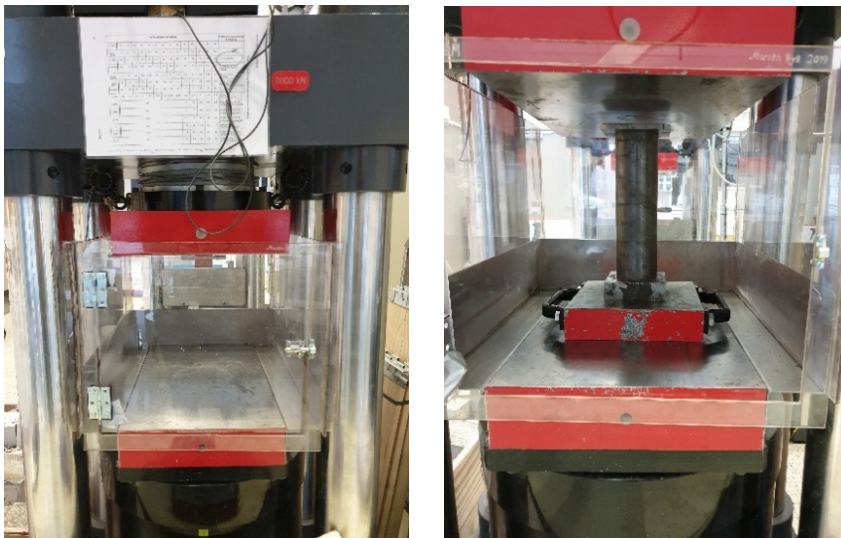


Figure 31: Test machine used for the stub column test

Preparation

The specimens were geometrically aligned in the test machine. The only readings from the test were load and vertical displacement provided by the test machine. No dial gages or electrical gages were used to get more accurate strain measurements. Next, the test speed was set to 10 kN/min for the intact specimens and 8 kN/min for the damaged ones. The standard requirement is a maximum loading rate of 21 MPa/min, corresponding to about 12.8 kN/min. Finally, the test was set to stop after a 10 kN drop in loading.

Testing

First, the two intact specimens were tested. After confirming good results, it was decided to induce rotated cracks on the remaining specimens. All the cracks on the column tests were placed parallel with the end surface. Hence, the wish to see the behaviors with rotated crack. One specimen was tested with a crack parallel to the end surface as a reference test. Further, two samples with a crack turned 45 degrees relative to the end surface were tested. As the specimens with rotated crack had about the same result, it was decided to put the crack perpendicular to the end surface on the last specimen.

4 Test result

4.1 Introduction

The results of the experiments, as described in Chapter 3, are reported in this chapter. First, the stub column test result is shown. Further, the column test and the cracked stub columns test results are reported. The end of the chapter covers a discussion of the results.

4.2 Stub-column test

As presented in Section 3.5, stub column tests are used to obtain the material properties by compressing short, intact columns until failure.

The yield strength was obtained by using the standard 0.2% strain offset method, first, by drawing a line with the same slope as the linear elastic part of the stress-strain curve. Next, the line was offset by 0.2% strain. Finally, the yield strength was found where the test curve and the line are crossing at **370 MPa**. The offset method is only used when the yield point is not a defined plateau dividing the elastic and plastic regime. The engineering stress strain curve corresponding to the stub column test is shown in Figure 32.

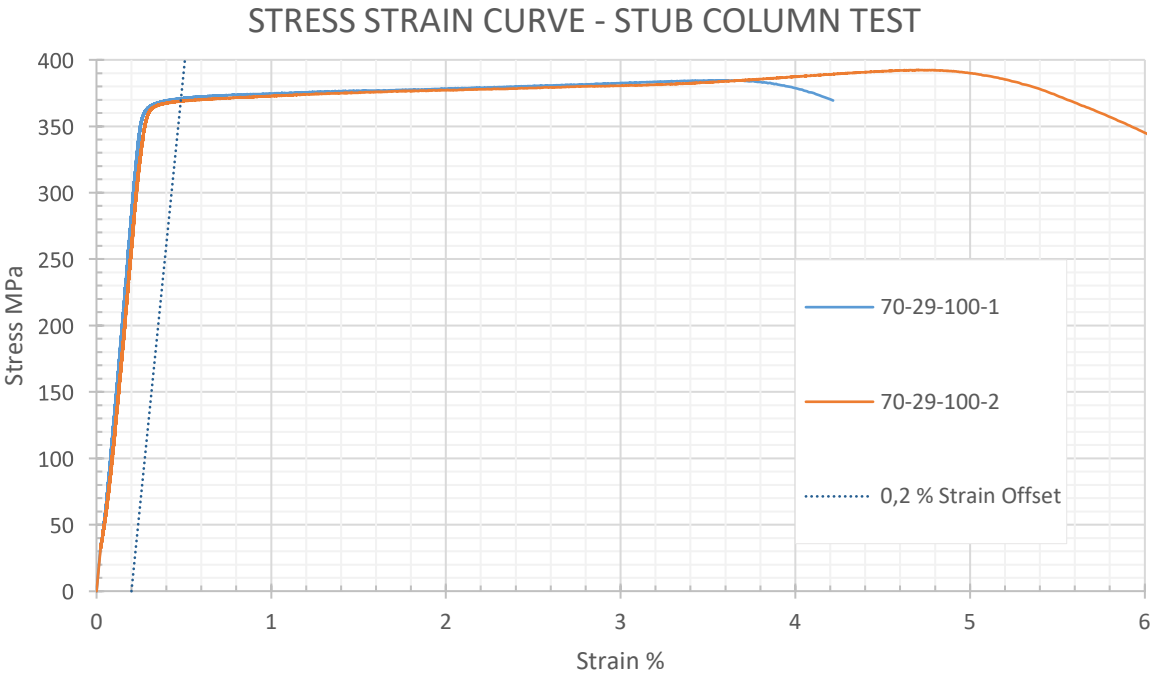


Figure 32: Stress strain curve, stub column test

An estimate of the specimens young's modulus was also obtained from the stress-strain curve by dividing delta stress by delta strain in region 150-250 MPa. The reason for choosing this region is the test settle at the beginning and the effect of residual stresses when the loading is getting larger. For more accurate determination of young's modulus. Better displacement measurements are needed.

Yield strength 370 MPa

Youngs modulus 150 GPa

The maximum load and deformed shape are shown in Table 1 and Figure 33 respectively.

Table 1: Maximum load intact stub column

Specimen	Maximum loading	Reference
70-29-100-1	235.15	S1
70-29-100-2	239.91	S2



Figure 33: Deformed shape stub columns

4.3 Column tests

4.3.1 Result column test - overview

The protocol below is an overview of all the column results. Figure 35 shows the max loading (failure load) of each specimen and the load-displacement curve of each specimen.

Parameter table:

Test protocol : Bachelor oppgave 2021
 Tester : Simen
 Creation date: 22.02.2021

Type strain extensometer:
 Machine data : Controller TT0322
 PistonStroke
 LoadCell 400 kN

Results:











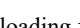
Legends	Nr	Date	ID	h mm	F _m kN
	1	24.02.2021	70-29-100-1	1500,0	208,95
	2	02.03.2021	70-29-88-1-UD	1500,0	203,75
	3	02.03.2021	70-29-76.5-1	1500,0	204,22
	4	02.03.2021	70-29-61.5-1	1500,0	210,70
	5	03.03.2021	70-29-88-2	1500,0	200,61
	6	04.03.2021	70-29-88-3-OD	1500,0	206,49
	7	04.03.2021	70-29-76.5-2-OD	1500,0	199,30
	8	04.03.2021	70-29-61.5-2-OD	1500,0	200,67
	9	05.03.2021	70-29-6-76.5-OD	1500,0	210,54
	10	05.03.2021	70-29-8-76.5-OD	1500,0	202,37
	11	05.03.2021	70-29-10-76.5-OD	1500,0	195,20

Figure 34: Max loading for test specimen

Series graphics:

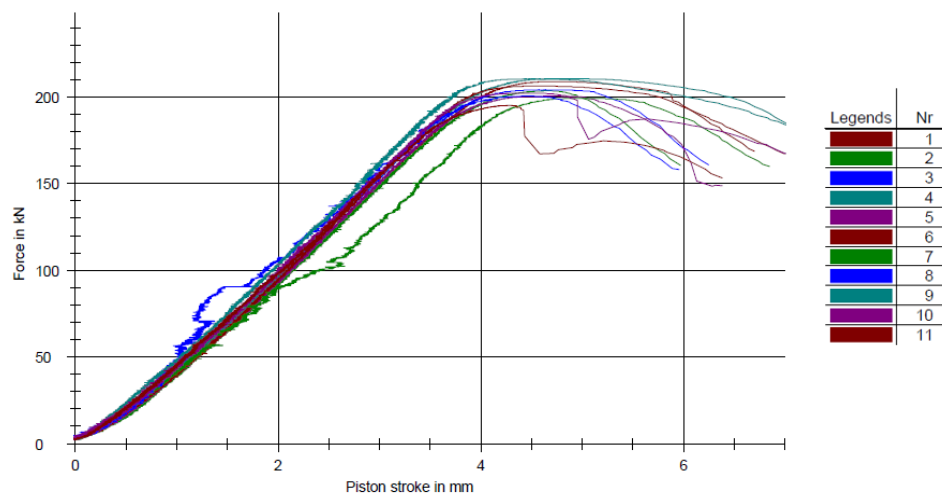


Figure 35: Load-displacement curve of each specimen

4.3.2 First five specimens

The test results of the first five specimens are shown in Table 2.

Table 2: Test results for first five specimen

Specimen	Maximum loading	Reference number for specimen
70-29-100	208.95 kN	1
70-29-4-88-1-UD	203.75 kN	2
70-29-4-88-2	200.61 kN	3
70-29-4-76.5-1	204.22 kN	4
70-29-4-61.5-1	210.70 kN	5

Specimen numbering indicate OD-thickness-remaining section area.
All the cracked specimens had 4 mm holes drilled in both crack tips.

The first specimen tested was an intact column, used as a control specimen, referenced as 70-29-100. This was followed by two specimens with the smallest crack size (88% remaining cross-sectional area), referenced as 70-29-88. The first of these specimens, identified UD, was placed upside down in the test machine and, hence, the crack was erroneously placed further up than intended. As a result, the test was re-run with a new specimen.

These were followed by the specimens with the medium crack and large crack size, representing 76.5% and 61.5% remaining section area respectively.

All the cracked specimens had the crack facing the same direction relative to the test machine and all the specimens buckled in the same direction, resulting in the cracks closing as shown in Figure 36 and Figure 37.

The erroneously placed specimen showed a higher capacity than the correct one, which confirms good placement of the crack. Hence, the test was decided to be included in the thesis.



Figure 36: Photo of first five specimens



Figure 37: Deformed shape of cracked area (small, medium and large crack respectively)

The load displacement curves for these five specimens are shown in Figure 38.

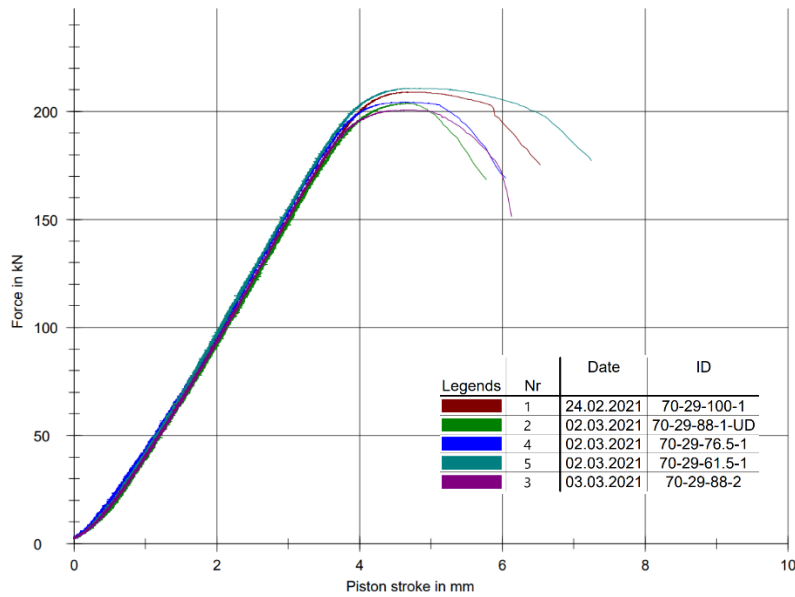


Figure 38: Load displacement curves for first five specimens

4.3.3 Rotated specimens

As previously mentioned, the first five specimens buckled in the same direction relative to the test machine. Hence, it was assumed that there could be an eccentricity in the test setup. To verify this, it was decided to test three more specimens with the same crack sizes (small, medium, and large) and rotate the specimen 180° relative to the testing machine. As expected, the buckling still happened in the same direction relative to the test machine, now opening the cracks. The resulting eccentricity observed from these experiments are further discussed in Section 4.6.1.

The maximum capacities of these three specimens are shown in Table 3, the deformed shape of these are shown in Figure 39, the local deformed shape around the crack is shown in Figure 40 and the load displacement curve in Figure 41.

Table 3: Test result rotated specimens

Specimen	Maximum loading	Reference number for specimen
70-29-4-88-3-OD	206.49 kN	6
70-29-4-76.5-2-OD	199.30 kN	7
70-29-4-61.5-2-OD	200.67 kN	8

Specimen numbering indicate OD-thickness-remaining section area.
All the cracked specimens had 4 mm holes drilled in both crack tips.

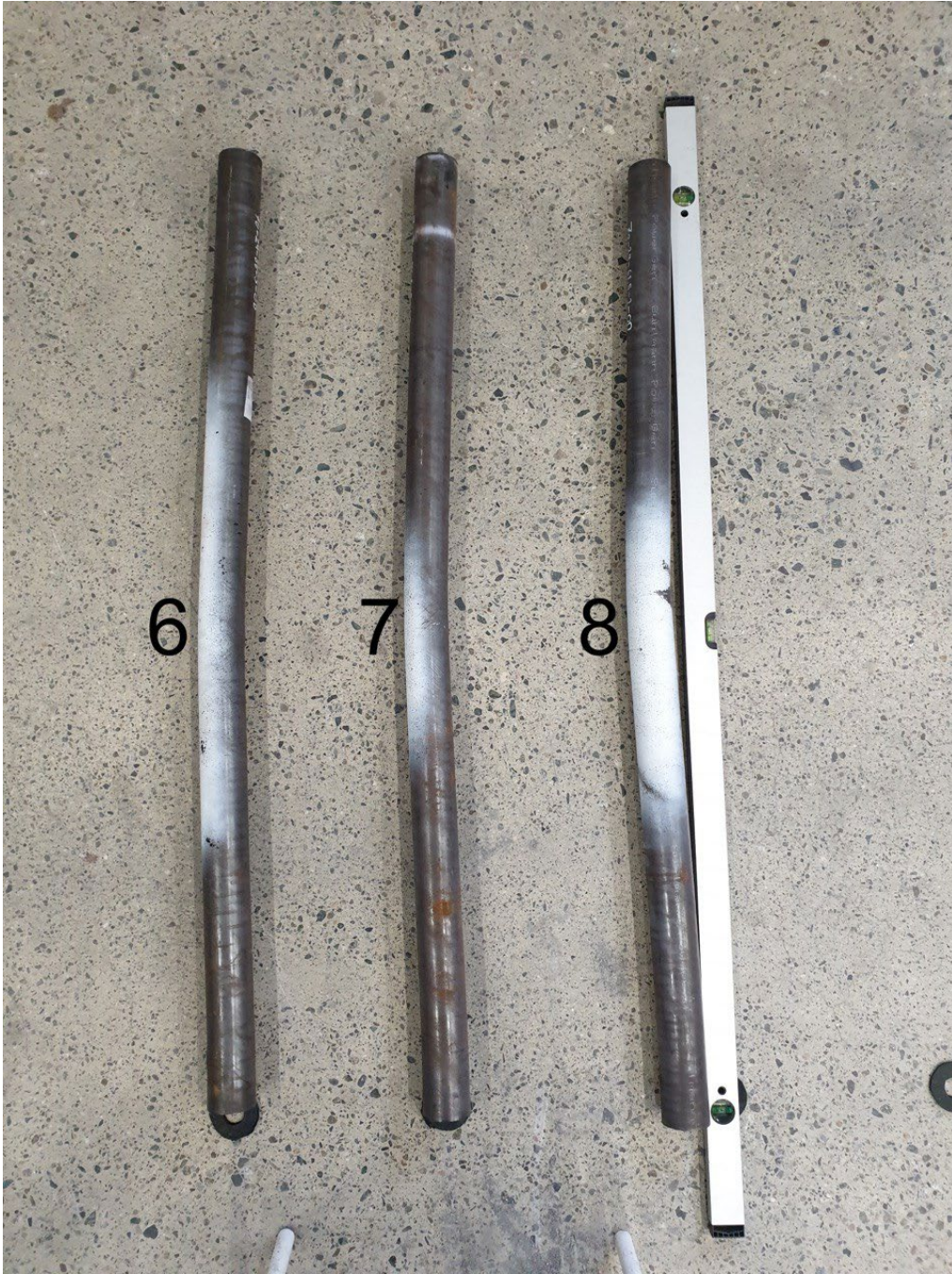


Figure 39: Photo of rotated specimens

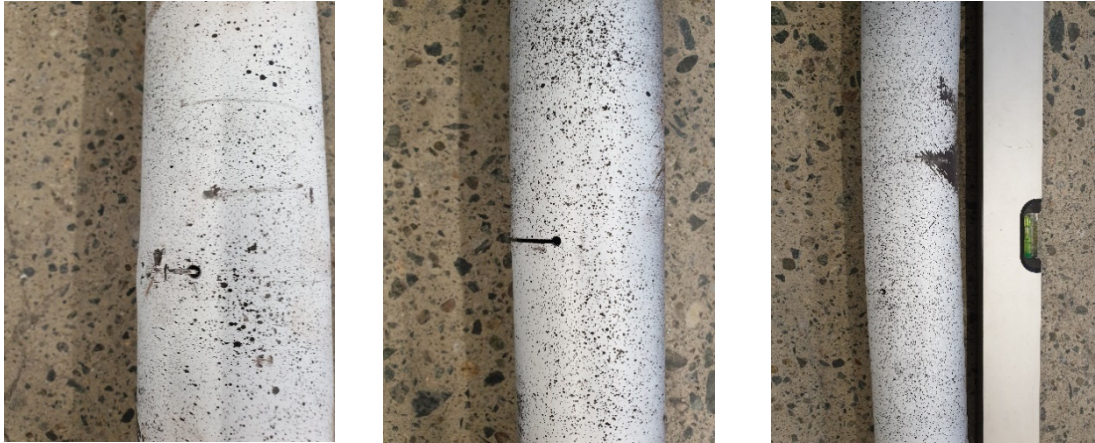


Figure 40: Deformed shape of cracked area (small, medium and large crack respectively)

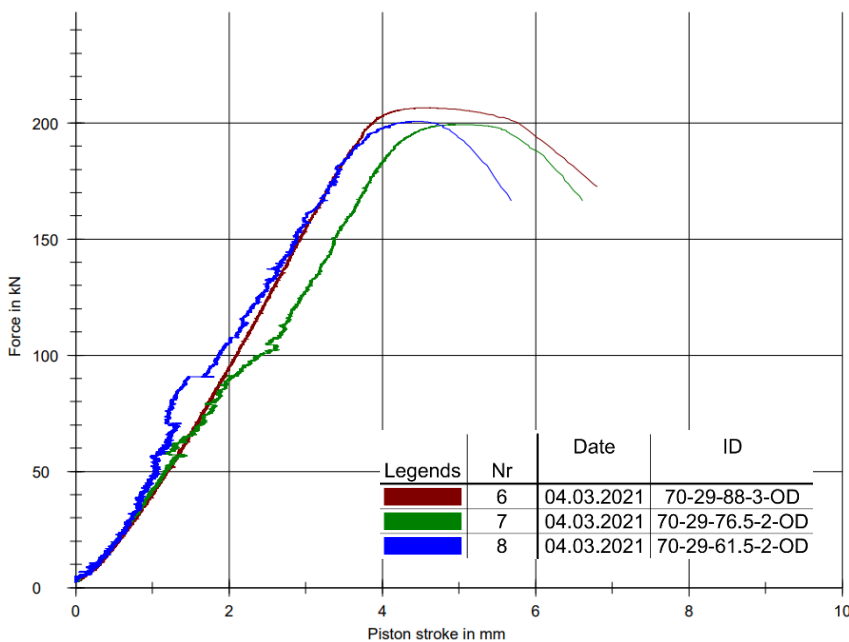


Figure 41: Load displacement curves for rotated specimens

4.3.4 Specimen with larger holes

The last three specimens were prepared with larger diameter holes, 6, 8 and 10 mm, but still maintaining the same crack length as for the first and second test set. The specimens were placed in a position where crack opening is expected, see Section 4.3.3.

The first specimen buckled in the same direction as all the other specimens as expected. In contrast, the last two specimens (8 and 10mm holes respectively) buckled the other direction and the crack closed. As mentioned previously, the issues relating to eccentricities will be further discussed in Section 4.6.1.

The maximum capacity of these specimens is shown in Table 4, the deformed shape and crack are displayed in Figure 42 and Figure 43, respectively, and the load displacement curve is shown in Figure 44.

Table 4: Test result specimen with larger holes

Specimen	Maximum loading	Reference number for specimen
70-29-6-76.5-OD	210.54 kN	9
70-29-8-76.5-OD	202.37 kN	10
70-29-10-76.5-OD	195.20 kN	11

Specimen numbering indicate OD-thickness-remaining section area.

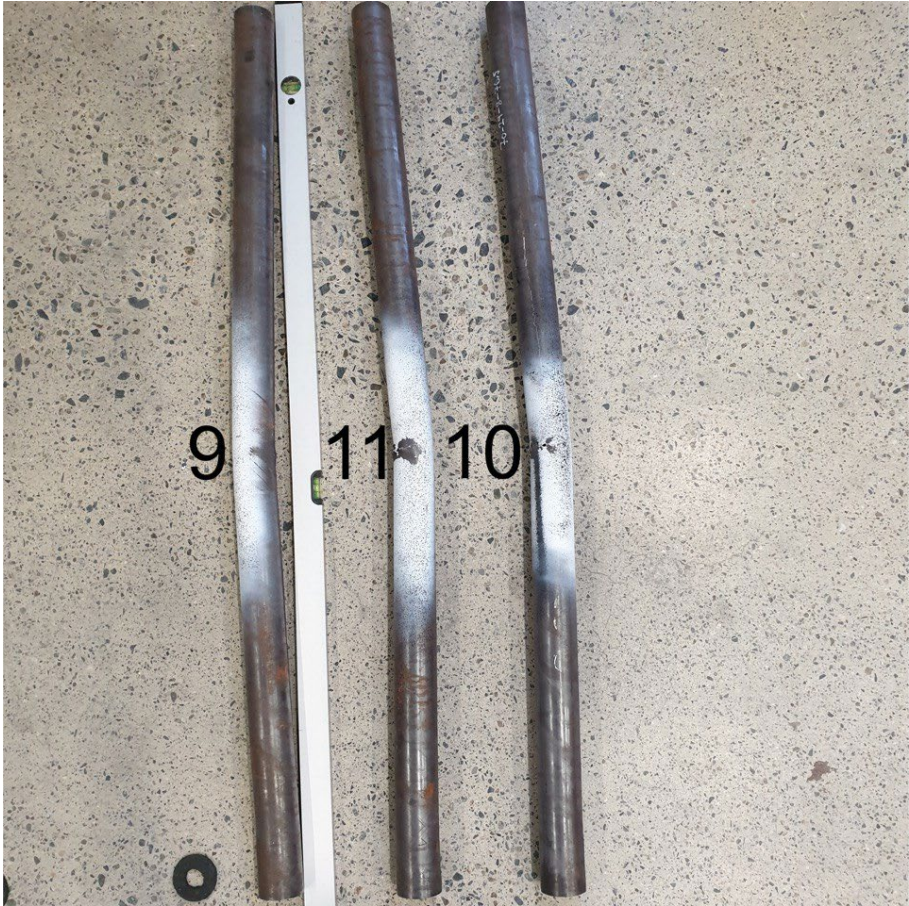


Figure 42: photo of specimens with larger holes



Figure 43: Deformed shape of cracked area (6, 8 and 10mm hole respectively)

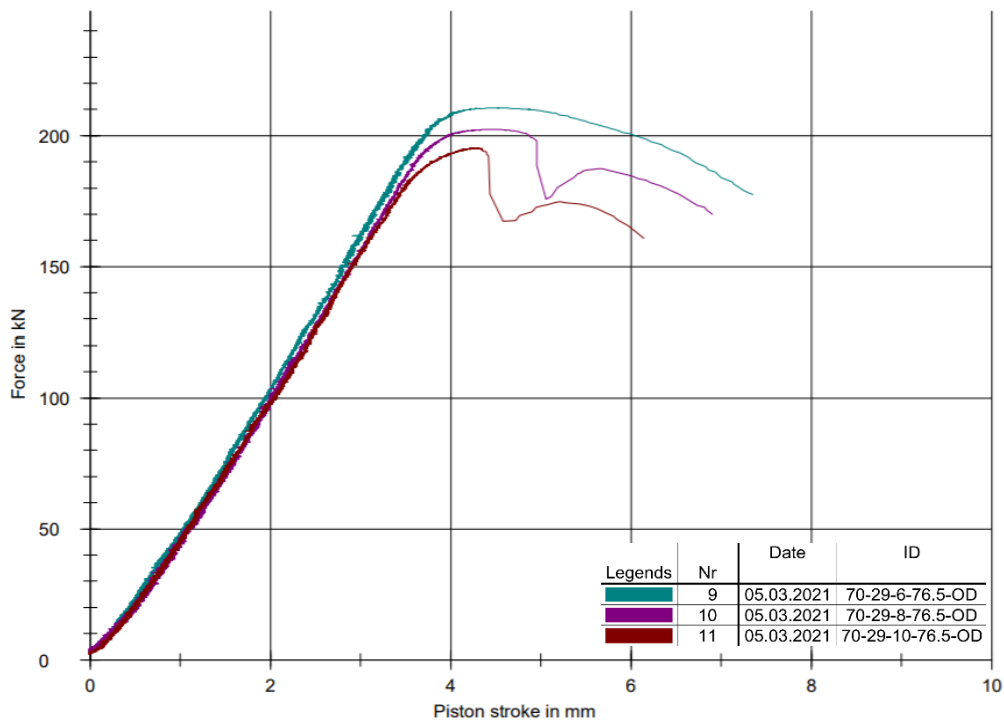


Figure 44: Load displacement curves specimen with larger holes

4.4 Cracked stub-column test results

All the column tests reported in Section 4.3 showed insignificant capacity reduction. To further study the effect of cracks in tubular members, angled cracks in stub columns were introduced.

The total stub column tests are shown in Table 5: Stub column tests results, including the specimens with no crack previously reported in Section 4.2. The 0° is included as a reference with identical crack to the full column tests.

Table 5: Stub column tests results

Specimen	Angle	Maximum loading	Reference
70-29-100-1	No crack	235.15 kN	S1
70-29-100-2	No crack	239.91 kN	S2
70-29-4-76.5-00-1	0°	235.42 kN	S3
70-29-4-76.5-45-1	45°	203.70 kN	S4
70-29-4-76.5-45-2	45°	202.32 kN	S5
70-29-4-76.5-90-1	90°	228.80 kN	S6

The engineering stress strain curves corresponding to the specimens are shown in Figure 46, and the deformed shape of the specimens in Figure 45.



Figure 45: Deformed shape stub columns

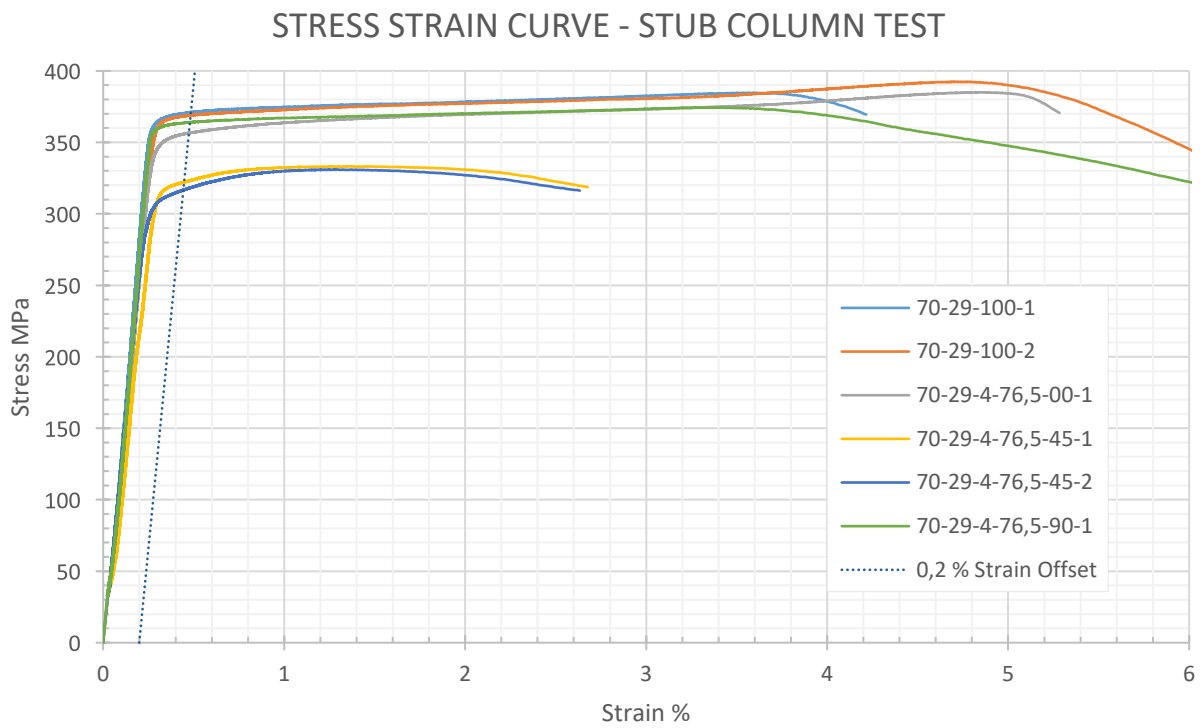


Figure 46: Stress strain curve stub column test

4.5 Discussion cracked stub-column test

As the results in Table 6 show, the 45° rotated crack gives a considerable reduction in capacity. The bearing effect on the crack surface is no longer present, and the deformed shape indicates a considerable amount of torsion present in the specimen. The specimen with a 90° degree crack showed a relatively small reduction. This reduction is assumed to be due to hoop stresses and removed material.

Table 6: Cracked stub column capacity and finite element calculation

Specimen	Reference	Maximum loading	Finite element
70-29-4-76.5-45-1	S4	203.70 kN	198.85 kN
70-29-4-76.5-45-2	S5	202.32 kN	198.85 kN
70-29-4-76.5-90-1	S6	228.80 kN	226.45 kN

The cracked stub column has been modeled in finite element software Abaqus:2020 in a separate master thesis project (Vågen 2021). As shown in Table 6, these values show a capacity close to the test results.

4.6 Discussion of column test results

4.6.1 Eccentricity

In normal condition, the crack and holes in an axial compression loaded tubular member will always close (assuming crack length $< \frac{1}{2}$ circumference). This is because of the local eccentricity present shown in Figure 47. However, this was not the test's behavior, which means it was an initial eccentricity present either in the test setup or the column geometry.

As the initial out of straightness regarding geometry was measured to be insignificant and most of the buckling happened in the same direction, eccentricity is assumed in the test setup shown in Figure 47: Normal condition local eccentricity.

Where:

e_{rig}	eccentricity in test setup and
e_{holes}	local eccentricity due to the holes
e_{tot}	total eccentricity

Another important observation is that the crack gave inconsiderable capacity reduction, which can be explained by the crack surface having a full bearing. For the specimens with the crack closing, the slipping effect explained in Section 3.3.1 does not occur before the post-buckling phase. Hence, the only capacity reduction is due to the holes, which implies that the local eccentricity in the damaged area is due to the holes only.

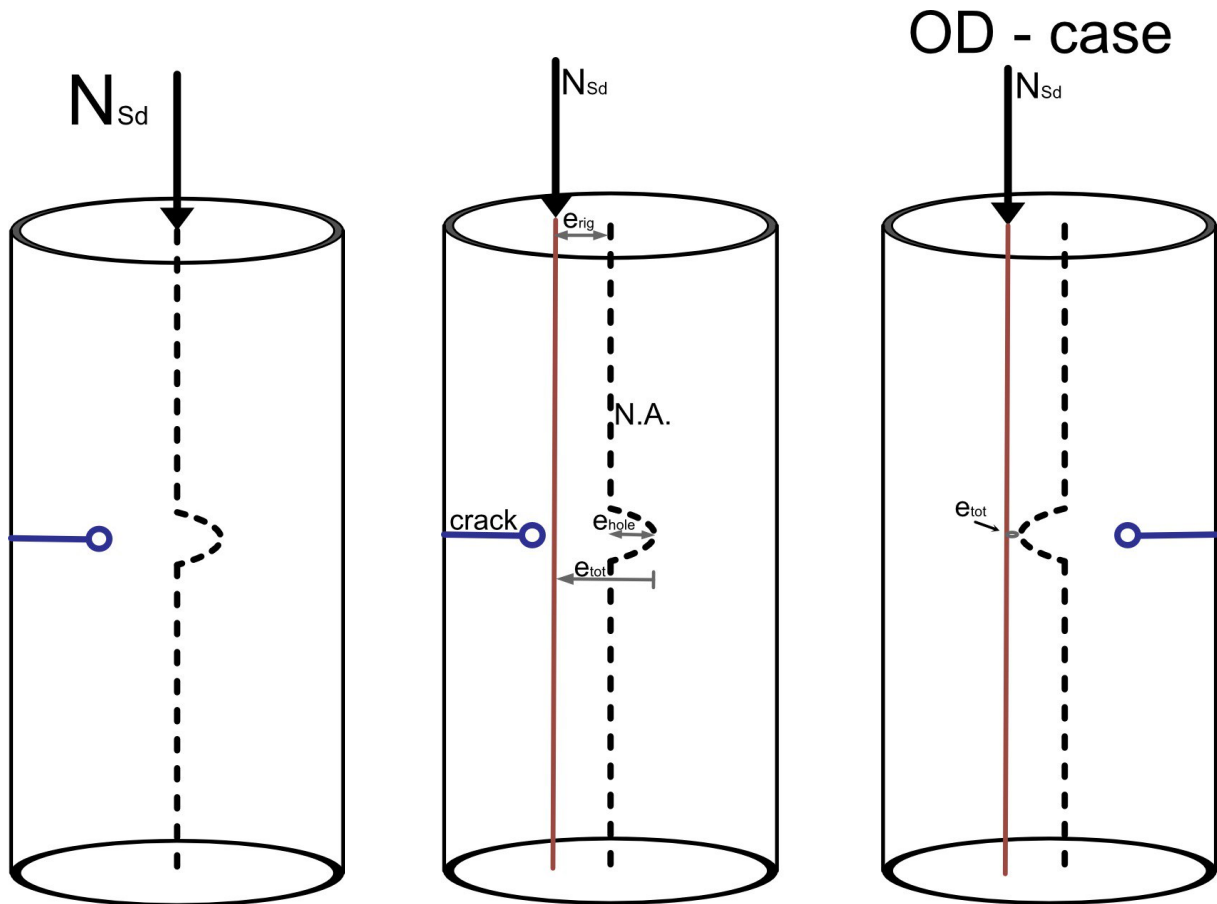


Figure 47: Normal condition local eccentricity and eccentricity due to holes and test setup, respectively

To be able to determine the axial capacity of the specimens, an estimate of the eccentricity in the test setup is needed. This can be done by studying the test result and the deformed column shapes. In Figure 48, all the rotated specimens are shown, which applies to the OD-case in Figure 47. In the OD-case $e_{tot} = e_{rig} - e_{hole}$ which give the following conditions:

Crack closing	$e_{rig} < e_{hole}$
Crack opening	$e_{rig} > e_{hole}$

For the crack to close, e_{hole} needs to be larger than the e_{rig} . This is happening in specimen nr. 10, with means $e_{rig} < e_{hole_{10}} = 2.1 \text{ mm}$. To determine the lower limit for e_{rig} specimen nr. 9 is considered, which have the largest e_{hole} , but still having the crack opening. Hence, $e_{rig} > e_{hole_{9}} = 1.5 \text{ mm}$. The result is as follow $1.5 \text{ mm} < e_{rig} < 2.1 \text{ mm}$

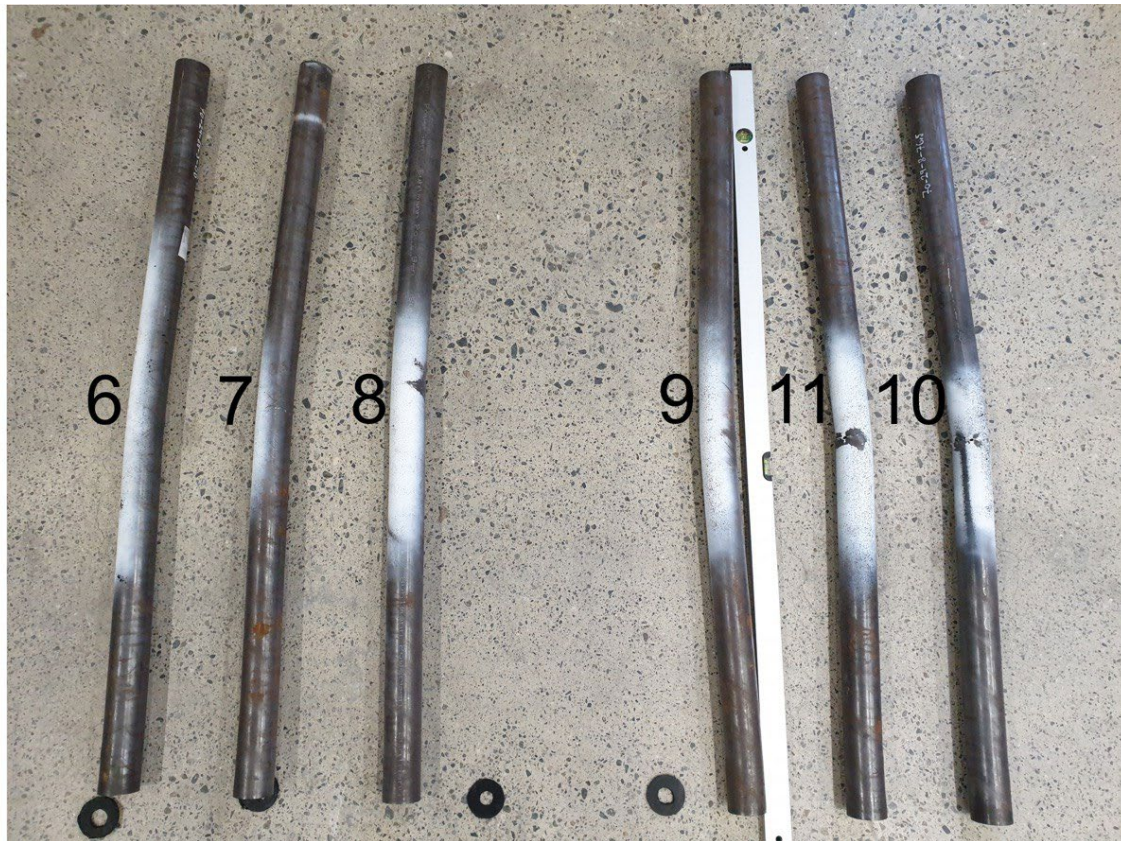


Figure 48: Rotated specimen identified as OD

4.6.2 Explaining results

As already discussed in section 4.6.1, the main differences in the capacity are due to the size and placement of the holes. The first four tests showed an increase in capacity as the crack size was getting larger, which is caused by the decrease in local eccentricity due to the holes getting closer to the neutral axis.

In contrast, the rotated specimens are more complicated to explain. As the eccentricity due to holes, in this case, is working against the eccentricity in the test setup, the expected capacity should be higher than in the first four cases. However, this wasn't the cases for all the specimens. Specimen 7 and 8 with medium and large crack size respectively had a lower capacity than 4 and 5, which have the same crack sizes but with the eccentricity due to the holes adding to eccentricity in the test setup. One explanation could be the reduced moment capacity in the cracked section due to the crack opening. However, this should not significantly affect the capacity as the specimens are in a range of slenderness where the moment capacity only becomes governing very close to failure. Another explanation could be found in the Load displacement curve in Figure 41, where there is an abnormal behavior. This behavior may be due to sliding in the cups or other deviations in the test setup or specimen, which results in a lower capacity.

When studying the deformed shapes, it was observed that some of the specimens buckled in a direction slightly of the hinge mechanism's direction, as shown in Figure 49. This behavior

could lead to a change in the effective length and the point with maximum stresses. Hence, possible discrepancies in the test result.

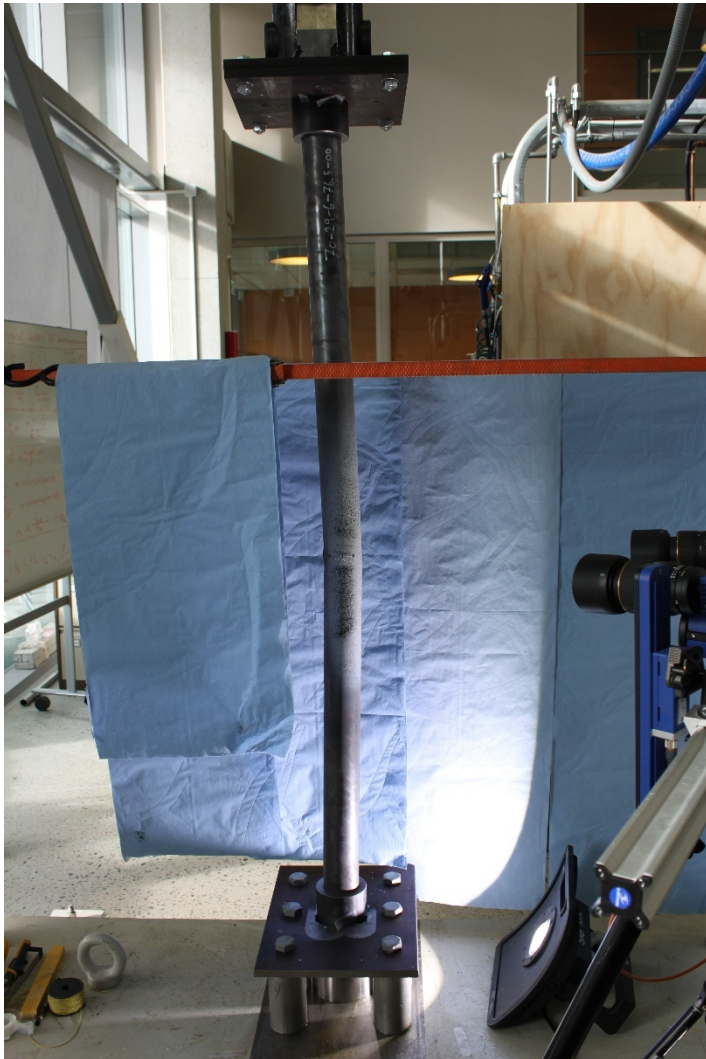


Figure 49: Deformed shape column

4.6.3 *DIC Discussion*

Unfortunately, the DIC did not provide any useful results and is therefore excluded from the thesis.

5 Comparison with analytical methods

5.1 Introduction

Several analytical methods exist to determine the axial capacity of a steel column. In this thesis, three commonly used approaches were used and compared with the experimental test results, namely:

- Empirical codified formulae commonly used in standards (e.g. NORSOK N-004 2004).
- Non-linear finite element analysis of the damaged column.
- Analytical formulae for column capacity (Perry-Robertson and Secant method).

5.2 Comparison with empirical codified formulae

The formulae in NORSOK N-004 2004, as presented in Section 2.5, were used as the empirical codified formulae to establish the unfactored capacity of the column. Further, the k-factor was set to 0.6 as the test result indicates both support acting somewhere between fixed and hinged. Using 0.6 instead of the theoretical k-factor is due to the considerable difference between the support condition in the test and the standard. The yield strength was set to 370 MPa, as obtained by the stub column tests.

Both pure compression and combined axial and bending have been evaluated. The bending moment is in these specimens caused by eccentricity due to the placement of the holes and the initial out of straightness imperfection of $L/2000$. However, as discussed in Section 4.6.1, the eccentricity in the rig itself was not included as this is a comparison with the standard design procedure.

Table 7: Values for tests and calculation according to NORSOK N-004.

Sample	Reference number	Damage position	f_u	f_y	Pu NORSOK		Pu exp
					Combined	Pure compression	
70-2.9-4-100-1	1	0	390	370	187.73	209.14	208.95
70-2.9-4-88-1-UD	2	705	390	370	174.82	195.96	203.75
70-2.9-4-88-2	3	795	390	370	174.82	195.96	200.61
70-2.9-4-88-3-OD	6	795	390	370	174.82	195.96	206.49
70-2.9-4-76.5-1	4	795	390	370	143.55	164.22	204.22
70-2.9-4-76.5-2-OD	7	795	390	370	143.55	164.22	199.30
70-2.9-4-61.5-1	5	795	390	370	91.70	114.48	210.70
70-2.9-4-61.5-2-OD	8	795	390	370	91.70	114.48	200.67
70-2.9-6-76.5-1-OD	9	795	390	370	139.20	164.22	210.54
70-2.9-8-76.5-1-OD	10	795	390	370	135.00	164.22	202.37
70-2.9-10-76.5-1-OD	11	795	390	370	130.93	164.22	195.20

1. Capacities calculated based on NORSOK N-004 is performed by eliminating the safety factors (all safety factors set to 1.0) and applying yield stress values of 370MPa from the stub-column tests of the pipe used in the tests. K-factor is set to 0.6. Eccentricity of the column due to fabrication misalignment is set to $L / 2000$ in these calculations.

As indicated in Figure 50, there is no correlation between the NORSOK capacity and the test results. This can be explained by the bearing effect on the crack surface described in Section 4.6.

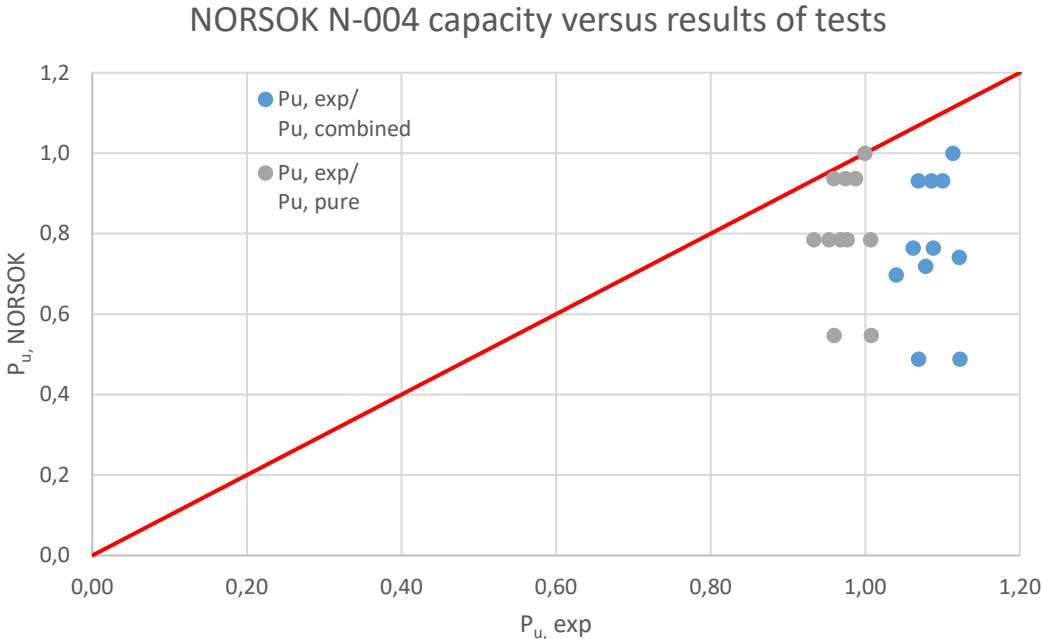


Figure 50: Comparison – test result and NORSOK N-004 calculation

The method for calculating the strength of cracked tubular members according to NORSOK N-004 is by first calculating a dent size corresponding to the crack. Next, The dent size is used to calculate reduction factors for axial and bending moment capacity ξ_c and ξ_M Respectively. These reduction factors are then used to calculate the slenderness ratio, axial and bending moment capacity. For the columns tested in this experiment, these reduction factors are too conservative. It is possible to get a more accurate calculation from NORSOK by customizing the calculation to the actual behavior. However, that will be unfortunate for the comparison. Hence, the standard design method is used.

5.3 Comparison with non-linear finite element models

The column tests have been modeled in the general finite element software Abaqus:2020 in a separate master thesis project (Vågen 2021). To be able to fit the model to the actual test, several adjustments have been made, as described in the following paragraphs.

Crack modeling

The columns were modeled only with holes; the crack was excluded. This is because bearing on the crack makes it behave close to an intact column, and a crack will give a too large capacity reduction. However, excluding the crack eliminates the potential moment reduction in the cracked section for the cases where the crack opened.

Support conditions

After studying the test result, the effective length factor, "k," could be estimated to be somewhere between 0.5 and 0.8, which means that fixed, hinged supports will give the most accurate effective length. However, the crack is located close to the middle of the column, which is far from the point where maximum stresses are expected with such supports. With a fixed, hinged setup, the maximum stresses under buckling should be closer to the hinge.

For the holes to have any considerable effect on the capacity in the model, either the crack and holes had to be moved, or the support condition had to be made equal. The solution was to make two models, one with hinged, hinged, and one fixed, fixed.

Imperfections

Several scenarios have been simulated with different imperfection factors. The result shown in Table 8 is based on an initial imperfection in the test setup at 1.5 mm

Table 8: Ultimate capacities for experimental tests and finite element method from Vågen (2021)

Sample	Reference number	Damage position	f_u	f_y	P_u (K = 0.5)	FE P_u (K = 1.0)	FE P_u exp
70-2.9-4-100-1	1	0	390	370	227.00	184.36	208.95
70-2.9-4-88-1-UD	2	705	390	370	220.42	177.21	203.75
70-2.9-4-88-2	3	795	390	370	220.42	177.21	200.61
70-2.9-4-88-3-OD	6	795	390	370	227.49	184.72	206.49
70-2.9-4-76.5-1	4	795	390	370	221.15	177.50	204.22
70-2.9-4-76.5-2-OD	7	795	390	370	227.17	184.70	199.30
70-2.9-4-61.5-1	5	795	390	370	223.70	178.07	210.70
70-2.9-4-61.5-2-OD	8	795	390	370	225.91	171.18	200.67

Capacities calculated in Finite element (ABAQUS) applying yield stress values of 370MPa from the stub-column tests of the pipe used in the tests. Eccentricity in the test setup is set to 1.6 mm

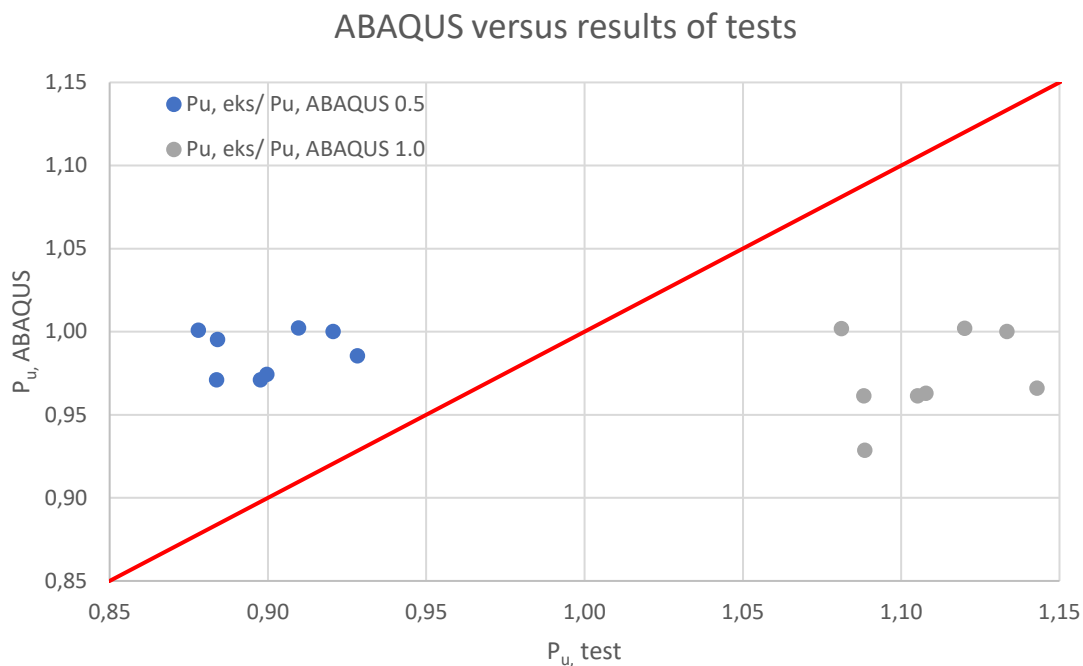


Figure 51: Comparison – test result and ABAQUS

As indicated in Figure 51, a k-factor of 1.0 is too large and 0.5 is too low. A rough interpolation indicates that the k factor is 0.6 - 0.7.

The buckled shape of the column in the finite element model with k factor 0.5 and 1.0 is shown in Figure 52.

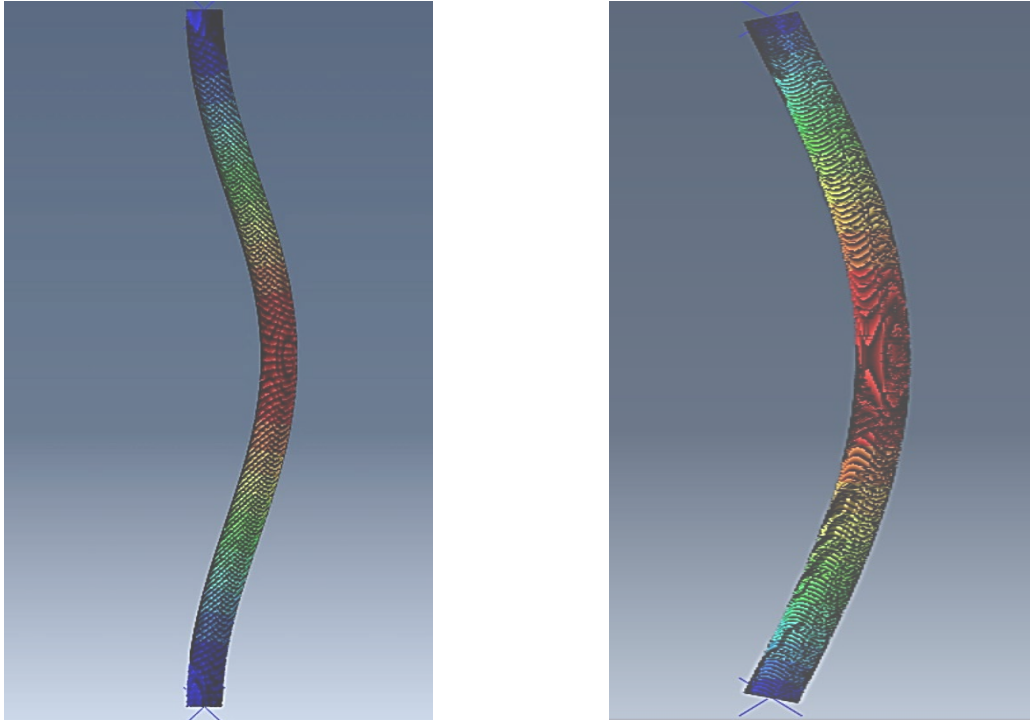


Figure 52: Finite element model of buckled shape with k factor 0.5 and 1.0, respectively (Vågen 2021)

5.4 Comparison with analytical models

5.4.1 Perry-Robertson formula

When calculating the axial capacity with the Perry Robertson formula presented in Section 2.3.2, the derivation bellow was used, which is the basis for the interaction formula in NORSOK N-004 for combined loading (bending moment and axial compression)

$$\frac{N}{N_{ULT}} + \frac{N(w_0 + e)}{M_{ULT} \left(1 - \frac{N}{N_E}\right)} \leq 1.0$$

In these calculations, the eccentricity in the test setup w_0 was set to 1.6 mm, which is explained in Section 4.6.1. When calculating the capacity of specimens 2-5, the eccentricity e due to the holes was added to the test setup eccentricity. For the rotated specimens, eccentricities due to the holes were subtracted from the eccentricities in the test setup.

Further, the plastic moment capacity was reduced only due to the holes in the cases where the crack closed. And for the cases where the crack opened, the moment capacity was reduced due to the crack. The reason behind the considerations in the calculation is explained in Section 4.6.

5.4.2 Secant formula

The secant formula calculation is based on the same consideration as the Perry Robertson calculation discussed in Section 5.4.1. The results from Perry Robertson and Secant formula are shown in Table 9.

Table 9: Ultimate capacities for experimental tests and calculation according to Perry Robertson and secant formula

Sample	Reference number	Damage position	f_u	f_y	Pu Perry (k factor =0.6)	Pu Secant	P_u Test
70-2.9-4-100-1	1	0	390	370	208.56	202.92	208.95
70-2.9-4-88-1-UP	2	705	390	370	192.29	183.27	203.75
70-2.9-4-88-2	3	795	390	370	192.29	183.27	200.61
70-2.9-4-88-3-OD	6	795	390	370	216.78	183.27	206.49
70-2.9-4-76.5-1	4	795	390	370	194.56	186.49	204.22
70-2.9-4-76.5-2-OD	7	795	390	370	211.12	186.49	199.30
70-2.9-4-61.5-1	5	795	390	370	199.46	192.91	210.70
70-2.9-4-61.5-2-OD	8	795	390	370	199.46	192.91	200.67
70-2.9-6-76.5-1-OD	9	795	390	370	219.26	187.50	210.54
70-2.9-8-76.5-1-OD	10	795	390	370	180.15	169.80	202.37
70-2.9-10-76.5-1-OD	11	795	390	370	172.71	161.19	195.20

Capacities calculated based on Perry Robertson equation and Secant formula, applying yield stress values of 370 MPa from the stub column tests of the pipe used in the tests. Eccentricity in the test setup is set to 1.6 mm

As shown in Figure 53, Perry Robertson gives the most accurate capacity calculation of the two analytical models. The secant formula provides a slightly lower capacity than Robertson. This is because the secant formula uses the elastic properties opposite to Robertson where the plastic properties are used. By introducing the elastic properties in the Robertson formula, the result will be exactly equal to the secant formula.

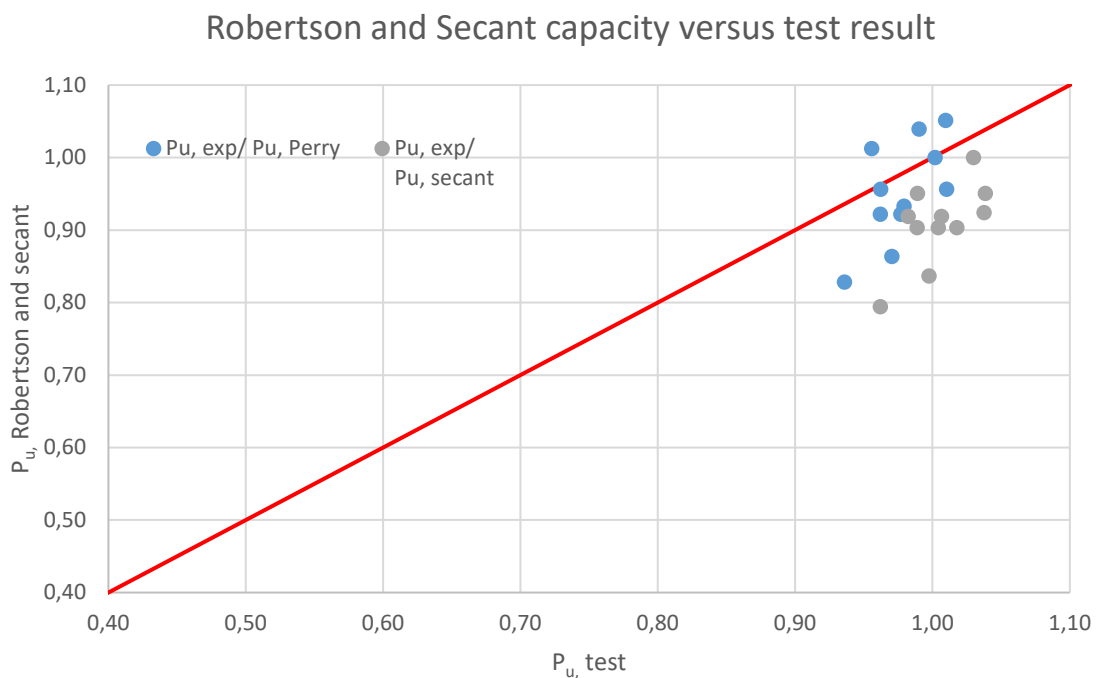


Figure 53: Comparison – test result and analytical models

5.5 Discussion of comparison

The result of the comparison as shown in Figure 54 indicates that the Perry Robertson formula provides the best approximation of the capacity. However, the deviation of the different methods from the test results, may be due to the following condition:

1. Assumptions in the calculations (e.g. boundary conditions)
2. Imperfection in test setup or specimens fabrication
3. Inaccuracies in the analytical and numerical calculation methods

However, It is assumed that the deviation from the calculation methods is insignificant, as all the methods are regarded as proven and well-established. The deviation regarding incorrect assumption is discussed in Sections 5.2 and 5.3.

The deviation in the Perry Robertson equation is assumed to be a result of imperfection in the test setup discussed in Section 4.6.1.

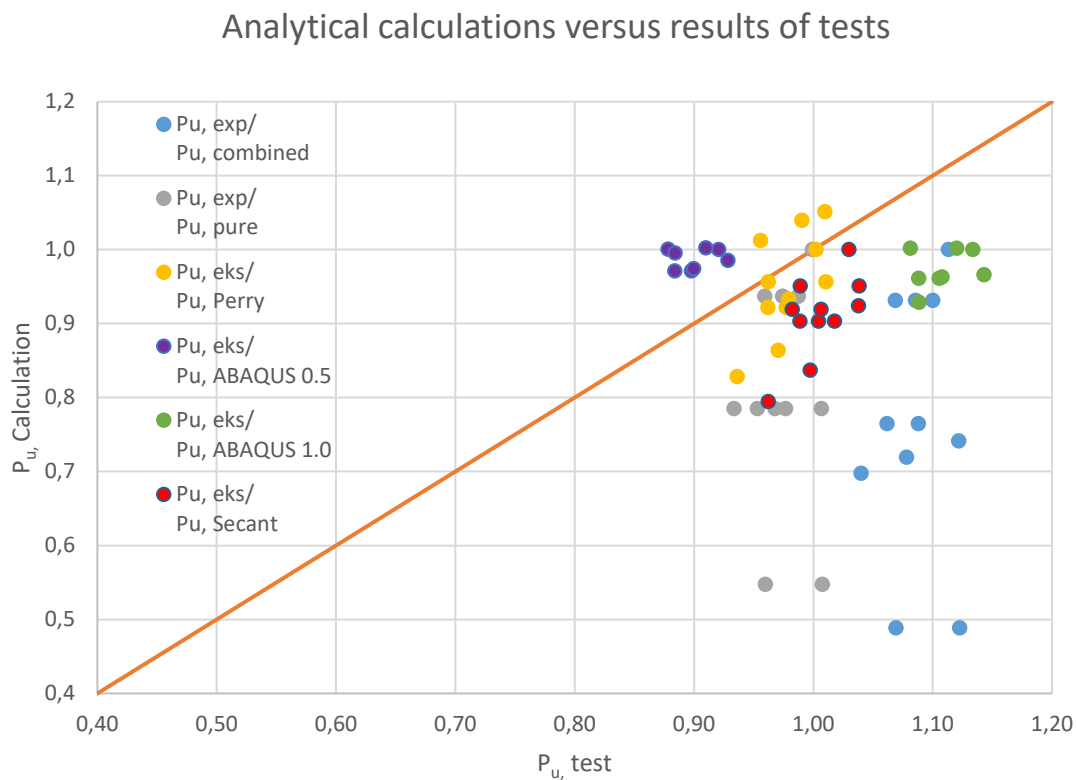


Figure 54: Comparison of the different analytical methods

6 Conclusion

The objective of the thesis is to experimentally study the effect of fatigue cracks on the capacity of tubular columns under axial compression. These are then compared to analytical methods, in addition to code check equations according to NORSOK N-004 (Standard Norge 2004) and non-linear FE analysis in a separate thesis (Vågen 2021).

The results of this study showed that cracks placed perpendicular to the direction of loading have an inconsiderable impact on the axial capacity due to full bearing on the crack surface. Hence, the NORSOK N-004 formulae have a very low correlation with the test result and provide a very conservative and inaccurate capacity calculation for columns under compression. Among the analytical calculation model presented in this thesis, Perry Robertson had the best correlation with the test results. This was expected as the calculation was best modified to the actual behavior of the columns tested.

To further study the effect of cracks in tubular members, angled cracks to the direction of loading in stub columns were introduced. The test results showed reduced axial capacity due to torsion and slipping of the crack surface, which indicated that angled cracks having a larger impact than straight cracks on the axial capacity of a tubular member.

There is no previous experimental research on the axial capacity of the cracked tubular member identified in this project. Hence, experimental tests were needed for better understanding the effect of fatigue cracks on tubular members and validate the existing NORSOK N-004 formulae. It was expected that cracks perpendicular to the load would significantly reduce axial compressive capacity, as shown in NORSOK N-004. However, the result indicated an inconsiderable reduction in capacity. Although this is an idealist experiment only considering pure compression with one type of slender columns, the results contribute to better insight on axial compression capacity of cracked tubular members.

The test performed in this thesis was limited to only axial compression loading, where the test machine limited the columns to a maximum diameter of 70 mm and 2m in height. For future work, it's recommended to introduce different loadings and mixed loadings, as fatigue crack is a result of cyclic loading where there are other loadings present than just pure compression. Furthermore, to better understand how cracks affect the capacity, future research could include angled cut on different locations on columns with various slenderness.

7 References

- AISC. (2005). Webinar A New Approach to Design for Stability. AISC. Retrieved from Webinar A New Approach to Design for Stability:
<https://www.aisc.org/education/continuingeducation/education-archives/a-new-approach-to-design-for-stability/>
- AISI. (2013). AISI S902-13 Stub-Column Test Method for Effective Area of Cold-Formed Steel Columns. American Iron and Steel Institute.
- Bmeafl. (2021, May 14). bmeafl. Retrieved from <https://bmeafl.com/category/laboratorium/>
- Britvec S. J., A. C. (1970). Effects of cold work in cold-formed steel structural members. Missouri: Missouri University of Science and Technology.
- DNV GL. (2015). DNVGL-CG-0128 Buckling. DNV GL.
- Ersdal, G., Sharp, J.V. and Stacey, A. (2019). Ageing and Life Extension of Offshore Structures. Wiley.
- Hebor, M. and Ricles, J. (1994). «Residual Strength and Repair of Corroded Marine Steel Tubulars,» ATLSS Report No. 94-10, ATLSS Eng. Research Center. Bethlehem, Pennsylvania: Lehigh University.
- Hibbeler, R. C. (2018). Chapter 13 Buckling of columns. In Mechanics of Materials (pp. 683-728). London: Pearson Educations.
- Lavision. (2021, May 14). Retrieved from www.lavision.de:
<https://www.lavision.de/en/techniques/dic-dvc/index.php>
- Mie.uth.gr. (2021, May 14). mie.uth.gr. Retrieved from <http://www.mie.uth.gr/labs/mex-lab/figureA9-7.html>
- Johnson, B.G. (1966) Guide to design criteria for metal compression members, Column Research Council, 2nd Ed. John Wiley and Sons, New York
- Osofero, A. I, Wadee, M.A. and Gardner, L. (2021, May 14). Numerical studies on the buckling resistance of prestressed stayed columns. Advances in structural engineering 16(3):487-498
- Ostapenko A, G. O. (1999). Tubular Columns with Multiple Corrosion Patches. Bethlehem: ATLSS Reports.
- Robertson, A. (1926). The strength of struts, Institution of Civil Engineers. London: Selected Engineering paper 28.
- Standard Norge (2004). NORSOK STANDARD N-004 Rev. 2, October 2004. Lysaker, Norway.

Standard Norge (2019). NS-EN 10217-1:2019. Lysaker, Norway.

Tubecon. (2021, May 14). Retrieved from <http://www.tubecon.co.za/en/technical-info/tubecon-wiki/mechanical-properties-of-common-steel.html>

Vo, T. and Hestholm, K. (2019). Buckling capacity of simulated patch corroded tubular columns – laboratory tests. Stavanger: University of Stavanger.

Vågen M. (2021). Master's thesis at the university of Stavanger (to be issued).

Warren, C. and Young, R.G. (n.d.). Solid Biomechanics. In Roark's Formulas for Stress and Strain (p. 976). New York: Mc Graw Hill.

Yong Bai, W.-l. J. (2015). Chapter 15 - Buckling/Collapse of Columns and Beam-Columns. In Y. Bai, Marine Structural Design (pp. 277-291). Elsevier Ltd.

Ziemian, R.D. (2010). Stability Design Criteria for Metal Structures. New Jersey: John Wiley and Sons, INC.

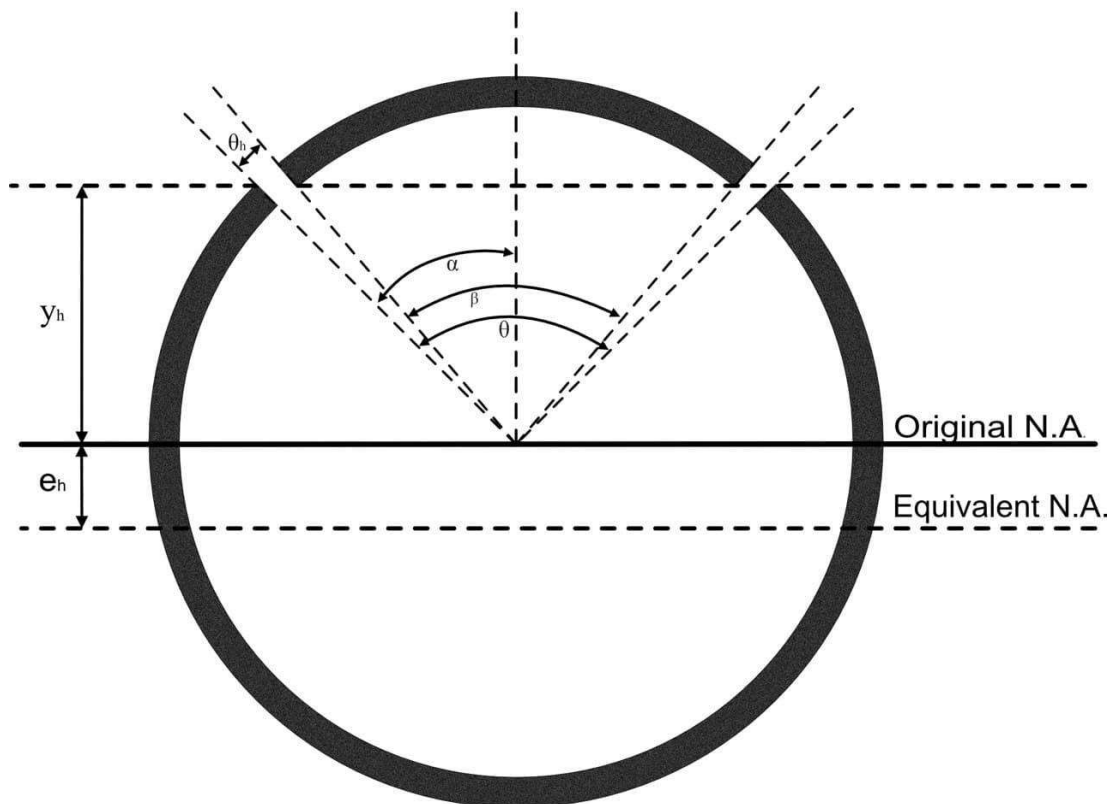
Appendices

Appendix 1 – NORSOK N-004 Calculation

CAPACITY OF CRACKED TUBULAR MEMBERS - NORSOK N-004

References

1. Lecture Notes
2. Roark's Formulas for Stress and Strain, 8th edition



Column section properties

<i>radius</i>	$r := 35\text{mm}$
<i>diameter</i>	$D := 2 \cdot r$
<i>thickness</i>	$t := 2.9\text{mm}$
<i>length</i>	$L_{ub} := 1.5\text{m}$
<i>effective length factor</i>	$k := 0.6$
<i>yield stress</i>	$f_y := 370\text{MPa}$
<i>young's modulus</i>	$E := 200\text{GPa}$
<i>partial factor</i>	$\gamma_M := 1$

original Section Properties

Original Area

$$A_o := 2\pi \left(r - \frac{t}{2} \right) t = 611.323 \cdot \text{mm}^2$$

Original moment of inertia

$$I_o := \frac{\pi}{4} \cdot \left[r^4 - (r-t)^4 \right] = 3.447 \times 10^5 \cdot \text{mm}^4$$

Radius of gyration

$$r_o := \sqrt{\frac{I_o}{A_o}}$$

Original elastic section modulus

$$W_o := \frac{I_o}{r} = 9.848 \times 10^3 \cdot \text{mm}^3$$

Plastic section modulus

$$Z_o := \frac{1}{6} \cdot \left[D^3 - (D-2t)^3 \right] = 1.307 \times 10^4 \cdot \text{mm}^3$$

max elastic moment intact section

$$M_{el.Rd} := f_y \cdot W_o$$

cracked section properties

remaining cross-section %

$$\%c := 76.5\%$$

crack size in rad

$$\theta_c := 2 \cdot \pi \cdot (100\% - \%c)$$

$$\alpha(\theta) := \frac{\theta}{2}$$

area crack

$$A_c(\theta) := t \cdot \left(r - \frac{t}{2} \right) \cdot \theta$$

centroided crack relativ to original N.A.

$$y_c(\theta) := \frac{2 \cdot \left(r - \frac{t}{2} \right) \cdot \sin(\alpha(\theta))}{\theta}$$

distance between original N.A and cracked section N.A.

$$e_c(\theta) := \frac{-A_c(\theta) \cdot y_c(\theta)}{A_o - A_c(\theta)}$$

moment of inertia of crack about centroid

$$I_{xc}(\theta) := r^3 \cdot t \cdot \left[\left(1 - \frac{3 \cdot t}{2 \cdot r} + \frac{t^2}{r^2} - \frac{t^3}{4 \cdot r^3} \right) \cdot \left[\alpha(\theta) + \sin(\alpha(\theta)) \cdot \cos(\alpha(\theta)) - \frac{2 \cdot (\sin(\alpha(\theta)))^2}{\alpha(\theta)} \right] \dots \right. \\ \left. + \frac{t^2 \cdot (\sin(\alpha(\theta)))^2}{3 \cdot r^2 \cdot \alpha(\theta) \left(2 - \frac{t}{r} \right)} \cdot \left(1 - \frac{t}{r} + \frac{t^2}{6 \cdot r^2} \right) \right]$$

moment of inertia
cracked section

$$I_c(\theta) := \left(I_o + A_o \cdot e_c(\theta)^2 \right) - \left[I_{xc}(\theta) + \left[A_c(\theta) \cdot (y_c(\theta) - e_c(\theta))^2 \right] \right]$$

largest distance between
N.A. and outer fiber

$$y_{\max}(\theta) := \begin{cases} \max(r \cdot \cos(\alpha(\theta)) - e_c(\theta), r + e_c(\theta)) & \text{if } \theta < \pi \\ \max[-e_c(\theta) + (r - t) \cdot \cos(\alpha(\theta)), r + e_c(\theta)] & \text{otherwise} \end{cases}$$

elastic section modulus
cracked section

$$W_c(\theta) := \frac{I_c(\theta)}{y_{\max}(\theta)}$$

max elastic moment
cracked section

$$M_{c,el.Rd}(\theta) := f_y \cdot W_c(\theta)$$

section with holes properties

hole size in mm

$$h := 4.1 \text{ mm}$$

hole size in rad

$$\theta_h := \frac{h}{r}$$

area hole

$$A_h := t \cdot \left(r - \frac{t}{2} \right) \cdot \theta_h$$

area section

$$A_{hs} := A_o - A_h$$

centroided holes relative
to original N.A

$$y_h(\theta) := \frac{(t - 2 \cdot r) \cdot (\sin(\alpha(\theta) - \theta_h) - \sin(\alpha(\theta)))}{2 \cdot \theta_h}$$

distance between original N.A
and sections with holes N.A

$$e_h(\theta) := \frac{2 \cdot A_h \cdot y_h(\theta)}{A_o - 2 \cdot A_h}$$

$$\beta(\theta) := \theta - 2 \cdot \theta_h$$

eccentricity due to holes

$$e_h(\theta_c) = 1.01 \cdot \text{mm}$$

moment of inertia
section with holes

$$I_h(\theta) := \left(I_o + A_o \cdot e_h(\theta)^2 \right) - \left[I_{xc}(\theta) + \left[A_c(\theta) \cdot (y_c(\theta) + e_h(\theta))^2 \right] \right] \dots \\ + \left[I_{xc}(\beta(\theta)) + \left[A_c(\beta(\theta)) \cdot (y_c(\beta(\theta)) + e_h(\theta))^2 \right] \right]$$

elastic section modulus
section with holes

$$W_h(\theta) := \frac{I_h(\theta)}{r}$$

NORSOK N-004 Intact Colum Equation 6.3.3

critical elastic buckling coefficient

$$C_e := 0.3$$

characteristic elastic local buckling strength

$$f_{cle} := 2 \cdot C_e \cdot E \cdot \frac{t}{D}$$

characteristic local buckling strength

$$f_{cl} := \begin{cases} f_y & \text{if } \frac{f_y}{f_{cle}} \leq 0.170 \\ \left[\left(1.047 - 0.274 \cdot \frac{f_y}{f_{cle}} \right) \cdot f_y \right] & \text{if } 0.170 < \frac{f_y}{f_{cle}} \leq 1.911 \\ f_{cle} & \text{if } \frac{f_y}{f_{cle}} > 1.911 \end{cases}$$

column slenderness parameter

$$\lambda_o := \frac{k \cdot L_{ub}}{\pi \cdot r_o} \sqrt{\frac{f_{cl}}{E}}$$

characteristic axial compressive strength

$$f_c := \begin{cases} \left[\left(1.0 - 0.28 \cdot \lambda_o^2 \right) \cdot f_y \right] & \text{if } \lambda_o \leq 1.34 = 342.103 \cdot \text{MPa} \\ \left(\frac{0.9}{\lambda_o} \cdot f_y \right) & \text{if } \lambda_o > 1.34 \end{cases}$$

member capacity

$$N_{cRd} := \frac{A_o \cdot f_c}{\gamma_M} = 209.136 \cdot \text{kN}$$

NORSOK N-004 Cracked Column Capacity

Equation 10.7.2 Equivalent dent depth

equivalent dent depth

$$\delta_c(\theta) := \frac{1}{2} \cdot \left(1 - \cos \left(\pi \cdot \frac{A_c(\theta)}{A_o} \right) \right) \cdot D$$

Equation 10.6.2.2 Dented tubular member

$$\xi_c(\theta) := \exp \left(-0.08 \cdot \frac{\delta_c(\theta)}{t} \right) \quad \frac{\delta_c(\theta_c)}{t} = 3.142$$

$$\xi_M(\theta) := \exp \left(-0.06 \cdot \frac{\delta_c(\theta)}{t} \right)$$

reduced slenderness of dented member

$$\lambda_d(\theta) := \frac{\xi_c(\theta)}{\xi_M(\theta)} \cdot \lambda_o$$

axial compressive
capacity
dent

$$N_{\text{dent}_c}(\theta) := \begin{cases} \left[(1.0 - 0.28 \cdot \lambda_d(\theta)^2) \cdot \xi_c(\theta) \cdot f_y \cdot A_o \right] & \text{if } \lambda_d(\theta) \leq 1.34 \\ \left(\frac{0.9}{\lambda_d(\theta)^2} \cdot \xi_c(\theta) \cdot f_y \cdot A_o \right) & \text{if } \lambda_d(\theta) > 1.34 \end{cases}$$

$$N_{\text{dent}_c_Rd} := \frac{N_{\text{dent}_c}(\theta_c)}{\gamma_M} = 164.215 \cdot \text{kN}$$

small crack size	$\theta_{88\%} := 2 \cdot \pi \cdot (100\% - 88\%)$
medium crack size	$\theta_{76.5\%} := 2 \cdot \pi \cdot (100\% - 76.5\%)$
large crack size	$\theta_{61.5\%} := 2 \cdot \pi \cdot (100\% - 61.5\%)$

Equation 10.6.2.3 Bending

characteristic bending strength

$$f_m := \begin{cases} \left(\frac{Z_o}{W_o} \cdot f_y \right) & \text{if } \frac{f_y \cdot D}{E \cdot t} \leq 0.0517 \\ \left[\left[1.13 - 2.58 \left(\frac{f_y \cdot D}{E \cdot t} \right) \right] \cdot \left(\frac{Z_o}{W_o} \cdot f_y \right) \right] & \text{if } 0.0517 < \frac{f_y \cdot D}{E \cdot t} \leq 0.1034 \\ \left[\left[0.94 - 0.76 \left(\frac{f_y \cdot D}{E \cdot t} \right) \right] \cdot \left(\frac{Z_o}{W_o} \cdot f_y \right) \right] & \text{if } 0.1034 < \frac{f_y \cdot D}{E \cdot t} \leq 120 \cdot \frac{f_y}{E} \end{cases}$$

bending moment capacity
dent section

$$M_{\text{dent}_Rd}(\theta) := \frac{f_m \cdot W_o \cdot \xi_M(\theta)}{\gamma_M}$$

Equation 10.6.2.4 Combined loading

euler buckling strength

$$N_{E_dent}(\theta) := \pi^2 \cdot \frac{E \cdot I_o \cdot \xi_M(\theta)}{(k \cdot L_{ub})^2}$$

eccentricity due to holes and initial out of straightness

$$\Delta y_2(\theta) := e_h(\theta) + \frac{L_{ub}}{2000}$$

$$\alpha_o(\theta) := 2 - 3 \cdot \frac{\delta_c(\theta)}{D}$$

$$f(N_{Sd}, \theta) := \frac{N_{Sd}}{N_{dent_c}(\theta)} + \sqrt{\left[\frac{N_{Sd} \cdot \Delta y_2(\theta)}{\left(1 - \frac{N_{Sd}}{N_{E_dent}(0.00001)}\right) \cdot M_{dent_Rd}(\theta)} \right]^{\alpha_o(\theta)}}$$

$$N_{Sd}(\theta) := \text{root}(f(N_{Sd}, \theta) - 1, N_{Sd}, 15\text{kN}, 250\text{kN})$$

Ultimate capacity calculation according to NORSOK N-004

capacity considering combined effect

capacity not considering combined effect

small crack size

$$N_{Sd}(\theta_{88\%}) = 174.82 \cdot \text{kN}$$

$$N_{dent_c}(\theta_{88\%}) = 195.957 \cdot \text{kN}$$

medium crack size

$$N_{Sd}(\theta_{76.5\%}) = 143.546 \cdot \text{kN}$$

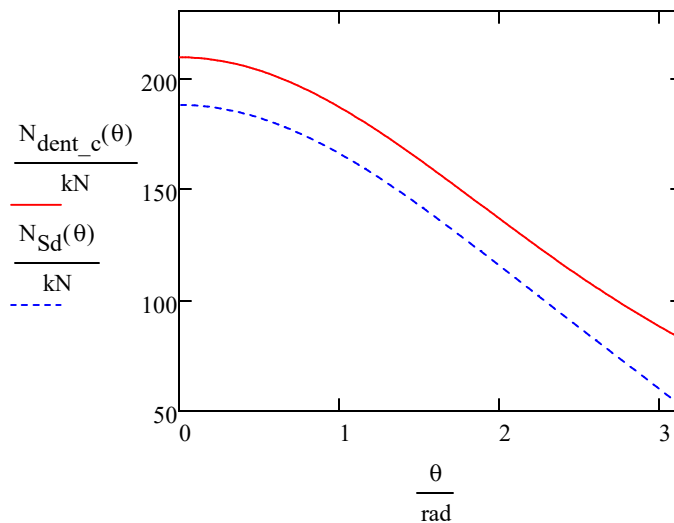
$$N_{dent_c}(\theta_{76.5\%}) = 164.215 \cdot \text{kN}$$

large crack size

$$N_{Sd}(\theta_{61.5\%}) = 91.703 \cdot \text{kN}$$

$$N_{dent_c}(\theta_{61.5\%}) = 114.477 \cdot \text{kN}$$

Ultimate capacity vs Crack sizes

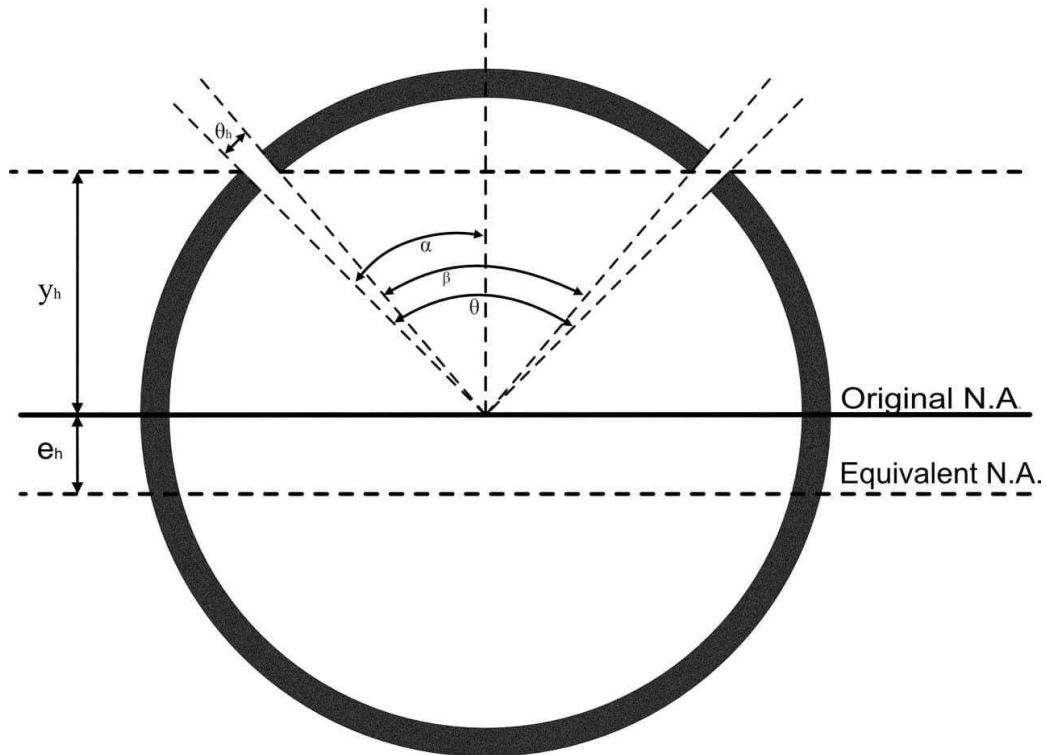


Appendix 2 – Perry Robertson and Secant Calculation

CAPACITY OF CRACKED TUBULAR MEMBERS - Perry Robertson, Secant

References

1. Lecture Notes
2. Roark's Formulas for Stress and Strain, 8th edition



Column section properties

<i>outer radius</i>	$r := 35\text{mm}$
<i>diameter</i>	$D := 2 \cdot r$
<i>thickness</i>	$t := 2.9\text{mm}$
<i>length</i>	$L_{ub} := 1.5\text{m}$
<i>effective length factor</i>	$k := 0.60$
<i>yield stress</i>	$f_y := 370\text{MPa}$
<i>young's modulus</i>	$E := 200\text{GPa}$

original Section Properties

Original Area	$A_o := 2\pi \left(r - \frac{t}{2} \right) t = 611.323 \cdot \text{mm}^2$
Original moment of inertia	$I_o := \frac{\pi}{4} \cdot [r^4 - (r-t)^4] = 3.447 \times 10^5 \cdot \text{mm}^4$
Radius of gyration	$r_o := \sqrt{\frac{I_o}{A_o}}$
slenderness ratio	$\lambda_o := \frac{L_{ub} \cdot k}{r_o} = 37.902$
Original elastic section modulus	$W_o := \frac{I_o}{r} = 9.848 \times 10^3 \cdot \text{mm}^3$
Plastic section modulus	$Z_o := \frac{1}{6} \cdot [D^3 - (D-2t)^3] = 1.307 \times 10^4 \cdot \text{mm}^3$
max elastic moment intact section	$M_{el.Rd} := f_y \cdot W_o$

cracked section properties

crack size in %	$\%c := 76.5\%$
crack size in rad	$\theta_c := 2 \cdot \pi \cdot (100\% - \%c)$
	$\alpha(\theta) := \frac{\theta}{2}$
area crack	$A_c(\theta) := t \cdot \left(r - \frac{t}{2} \right) \cdot \theta$
centroied carck relativ to original N.A.	$y_c(\theta) := \frac{2 \cdot \left(r - \frac{t}{2} \right) \cdot \sin(\alpha(\theta))}{\theta}$
distance between original N.A and cracked section N.A.	$e_c(\theta) := \frac{-A_c(\theta) \cdot y_c(\theta)}{A_o - A_c(\theta)}$

*moment of inertia of crack
about centroid*

$$I_{xc}(\theta) := r^3 \cdot t \cdot \left[\left(1 - \frac{3 \cdot t}{2 \cdot r} + \frac{t^2}{r^2} - \frac{t^3}{4 \cdot r^3} \right) \cdot \left[\alpha(\theta) + \sin(\alpha(\theta)) \cdot \cos(\alpha(\theta)) - \frac{2 \cdot (\sin(\alpha(\theta)))^2}{\alpha(\theta)} \right] \dots \right. \\ \left. + \frac{t^2 \cdot (\sin(\alpha(\theta)))^2}{3 \cdot r^2 \cdot \alpha(\theta) \left(2 - \frac{t}{r} \right)} \cdot \left(1 - \frac{t}{r} + \frac{t^2}{6 \cdot r^2} \right) \right]$$

*moment of inertia
cracked section*

$$I_c(\theta) := \left(I_o + A_o \cdot e_c(\theta)^2 \right) - \left[I_{xc}(\theta) + \left[A_c(\theta) \cdot (y_c(\theta) - e_c(\theta))^2 \right] \right]$$

*largest distance between
N.A. and outer fiber*

$$y_{\max}(\theta) := \begin{cases} \max(r \cdot \cos(\alpha(\theta)) - e_c(\theta), r + e_c(\theta)) & \text{if } \theta < \pi \\ \max[-e_c(\theta) + (r - t) \cdot \cos(\alpha(\theta)), r + e_c(\theta)] & \text{otherwise} \end{cases}$$

*elastic section modulus
cracked section*

$$W_c(\theta) := \frac{I_c(\theta)}{y_{\max}(\theta)}$$

*max elastic moment
cracked section*

$$M_{c_{el.Rd}}(\theta) := f_y \cdot W_c(\theta)$$

Plastic section modulus crack

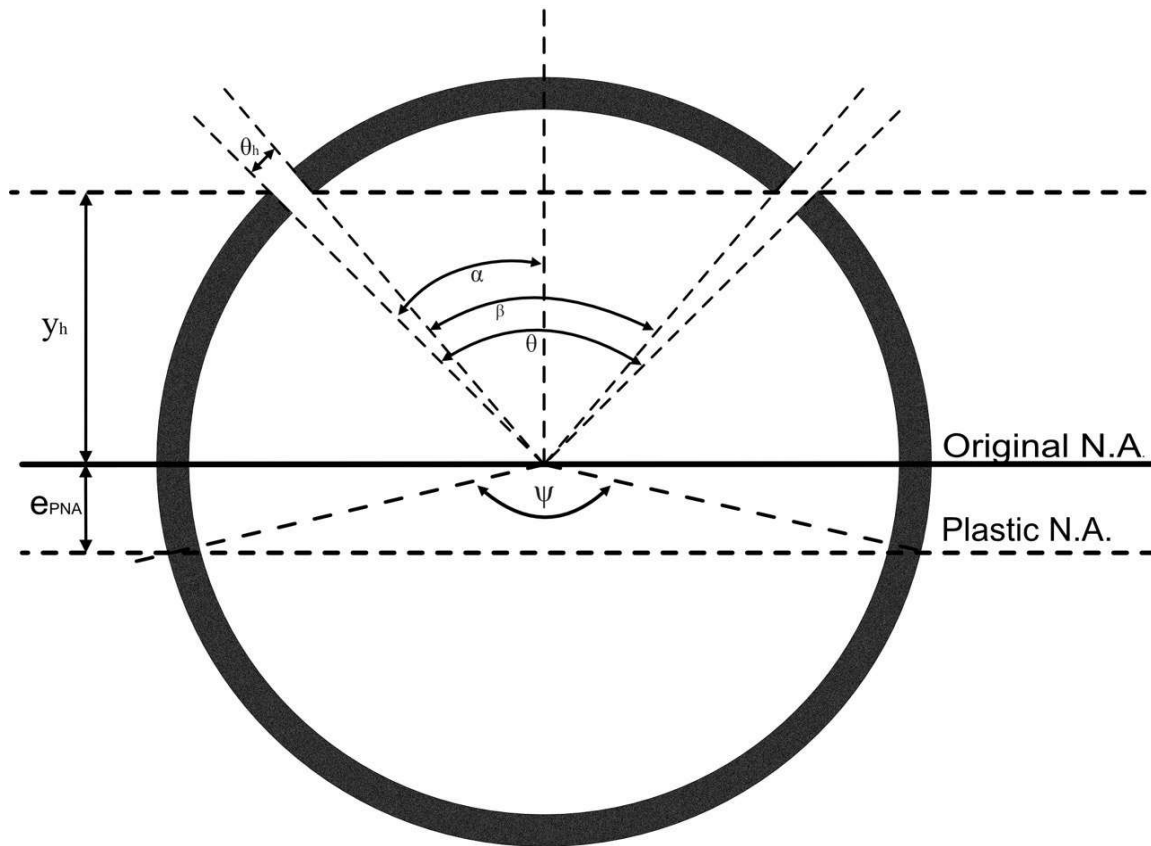
$$\begin{aligned} \psi(\theta) &:= \pi - \alpha(\theta) & e_{pna}(\theta) &:= r \cdot \cos\left(\frac{\psi(\theta)}{2}\right) \\ S_c(\theta) &:= \theta \cdot r \\ A_1(\theta) &:= t \cdot \left(r - \frac{t}{2} \right) \cdot (2 \cdot \pi - \psi(\theta) - \theta) & y_{p2}(\theta) &:= \frac{-\sin\left(\frac{\psi(\theta)}{2}\right) \cdot (t - 2 \cdot r)}{\psi(\theta)} \\ A_2(\theta) &:= \psi(\theta) \cdot t \cdot \left(r - \frac{t}{2} \right) & y_2(\theta) &:= y_{p2}(\theta) - e_{pna}(\theta) \end{aligned}$$

$$y_{p1}(\theta) := \frac{-A_c(\theta) \cdot y_c(\theta) - \psi(\theta) \cdot t \cdot \left(r - \frac{t}{2} \right) \cdot (-y_{p2}(\theta))}{A_1(\theta)}$$

$$y_1(\theta) := y_{p1}(\theta) + e_{pna}(\theta)$$

*plastic section modulus
crack*

$$W_{c_{pl}}(\theta) := A_1(\theta) \cdot y_1(\theta) + A_2(\theta) \cdot y_2(\theta)$$



section with holes properties

hole size in mm

$$h := 4.1\text{mm}$$

hole size in rad

$$\theta_h := \frac{h}{r}$$

area hole

$$A_h := t \cdot \left(r - \frac{t}{2} \right) \cdot \theta_h$$

area section

$$A_{hs} := A_o - A_h$$

centroided holes relative to original N.A

$$y_h(\theta) := \frac{(t - 2 \cdot r) \cdot (\sin(\alpha(\theta) - \theta_h) - \sin(\alpha(\theta)))}{2 \cdot \theta_h}$$

distance between original N.A and sections with holes N.A

$$e_h(\theta) := \frac{2 \cdot A_h \cdot y_h(\theta)}{A_o - 2 \cdot A_h}$$

$$\beta(\theta) := \theta - 2 \cdot \theta_h$$

eccentricity due to holes

$$e_h(\theta_c) = 1.01 \cdot \text{mm}$$

*moment of inertia
section with holes*

$$I_h(\theta) := \left(I_o + A_o \cdot e_h(\theta)^2 \right) - \left[I_{xc}(\theta) + \left[A_c(\theta) \cdot (y_c(\theta) + e_h(\theta))^2 \right] \right] \dots \\ + \left[I_{xc}(\beta(\theta)) + \left[A_c(\beta(\theta)) \cdot (y_c(\beta(\theta)) + e_h(\theta))^2 \right] \right]$$

*elastic section modulus
section with holes*

$$W_h(\theta) := \frac{I_h(\theta)}{r}$$

*max elastic moment
section with holes*

$$M_{h_el.Rd}(\theta) := W_h(\theta) \cdot f_y$$

*eccentricity needed
to get tension in crack*

$$e_{test}(\theta) := \frac{-W_h(\theta)}{A_{hs}}$$

Plastic section modulus holes onley

$$\psi_h := \pi - \theta_h$$

$$e_{h_pna} := r \cdot \cos\left(\frac{\psi_h}{2}\right)$$

$$S_h(\theta) := \theta \cdot r$$

$$y_{h_p2} := \frac{-\sin\left(\frac{\psi_h}{2}\right) \cdot (t - 2 \cdot r)}{\psi_h}$$

$$A_{h2} := \psi_h \cdot t \cdot \left(r - \frac{t}{2} \right)$$

$$A_{h1} := A_o - A_{h2} - 2 \cdot A_h$$

$$y_{h_2} := y_{h_p2} - e_{h_pna}$$

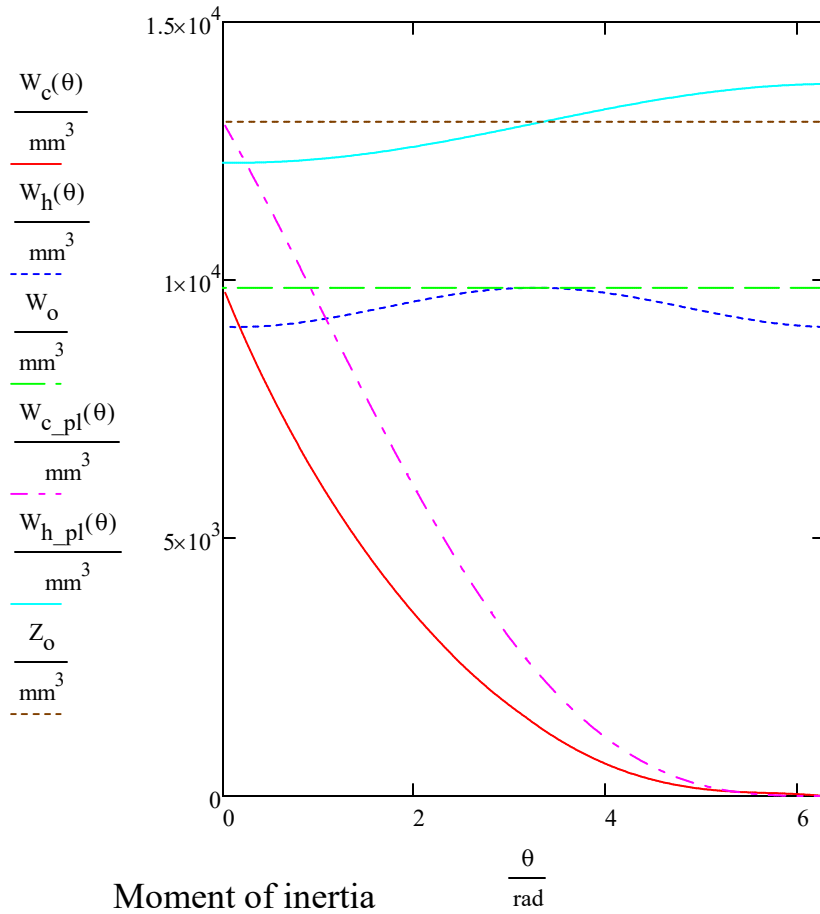
$$y_{hp1}(\theta) := \frac{-2 \cdot A_h \cdot y_h(\theta) + A_{h1} \cdot y_{h_p2}}{A_{h1}}$$

$$y_{h_1}(\theta) := y_{hp1}(\theta) + e_{h_pna}$$

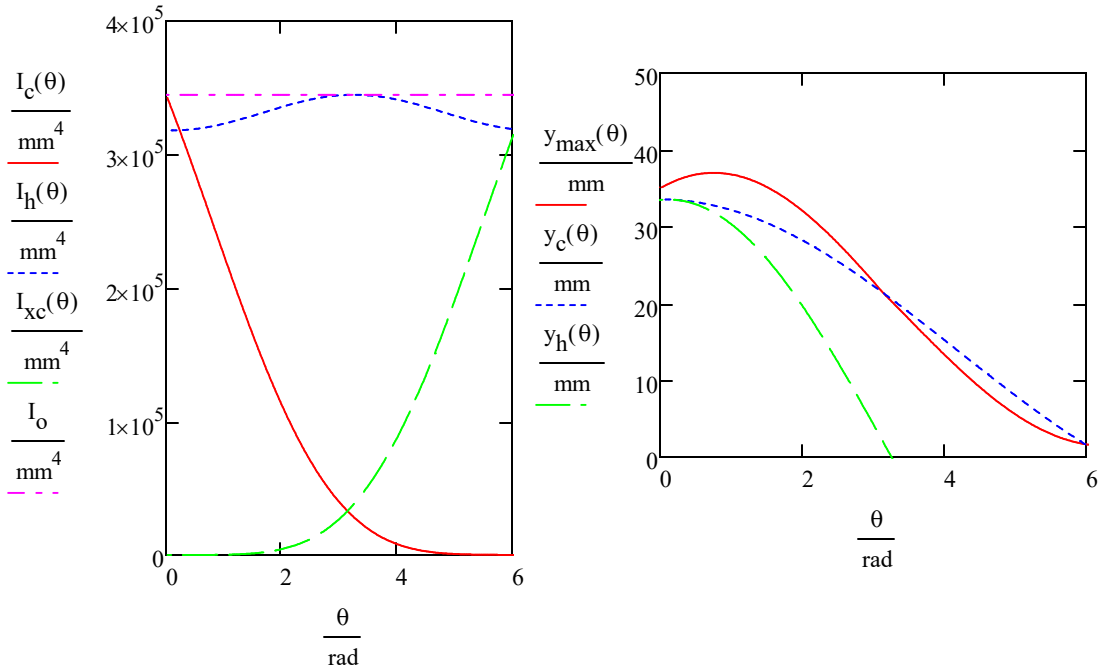
*plastic section modulus
crack*

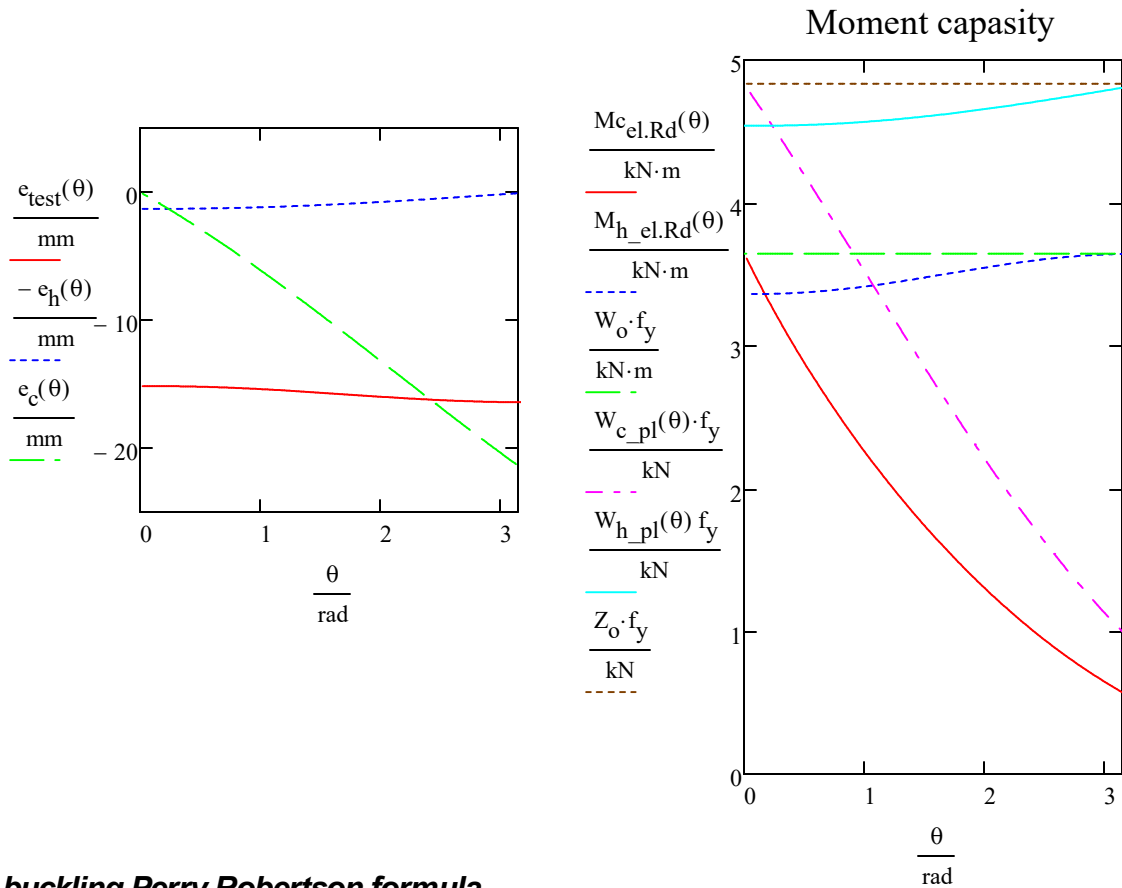
$$W_{h_p1}(\theta) := A_{h1} \cdot y_{h_1}(\theta) + A_{h2} \cdot y_{h_2} \quad \text{only for } \theta < \pi$$

Section modulus



Moment of inertia





buckling Perry Robertson formula

Crack closes - considering reduced capacity onley due to holes

radius of gyration $r_{gh}(\theta) := \sqrt{\frac{I_h(\theta)}{A_{hs}}}$ *small crack size* $\theta_{88\%} := 2 \cdot \pi \cdot (100\% - 88\%)$

Euler buckling reduced due to holes $N_e(\theta) := \frac{E \cdot \pi^2 \cdot A_{hs}}{\left(\frac{L_{ub} \cdot k}{r_{gh}(\theta)}\right)^2}$ *medium crack size* $\theta_{76.5\%} := 2 \cdot \pi \cdot (100\% - 76.5\%)$

Euler Buckling load $N_E := \frac{E \cdot \pi^2 \cdot A_o}{\left(\frac{L_{ub} \cdot k}{r}\right)^2}$ *large crack size* $\theta_{61.5\%} := 2 \cdot \pi \cdot (100\% - 61.5\%)$

eccentricity test setup $e_o := 1.6mm$

total eccentricity $e_{\text{tot}}(\theta) := |e_o + e_h(\theta)|$

ultimate axial capacity $N_d := A_{\text{hs}} \cdot f_y = 2.22 \times 10^5 \text{ N}$

Perry Roberston formula
$$f(N_{\text{pr}}, \theta) := \frac{N_{\text{pr}}}{N_d} + \frac{N_{\text{pr}} \cdot (e_{\text{tot}}(\theta)) \cdot \left(\frac{1}{1 - \frac{N_{\text{pr}}}{N_E}} \right)}{W_{\text{h_pl}}(\theta) \cdot f_y}$$

solve equation for 1 $N_{\text{pr}}(\theta) := \text{root}(f(N_{\text{pr}}, \theta) - 1, N_{\text{pr}}, 10\text{kN}, 300\text{kN})$

small crack size $N_{\text{pr}}(\theta_{88\%}) = 192.289 \cdot \text{kN}$

medium crack size $N_{\text{pr}}(\theta_{76.5\%}) = 194.56 \cdot \text{kN}$

large crack size $N_{\text{pr}}(\theta_{61.5\%}) = 199.485 \cdot \text{kN}$

Crack opening - considering reduced moment capacity due to crack

total eccentricity $e_{o_tot}(\theta) := |e_o - e_h(\theta)|$

Perry Roberston formula
$$f_o(N_{o_pr}, \theta) := \frac{N_{o_pr}}{N_d} + \frac{N_{o_pr} \cdot (e_{o_tot}(\theta)) \cdot \left(\frac{1}{1 - \frac{N_{o_pr}}{N_E}} \right)}{W_{c_pl}(\theta) \cdot f_y}$$

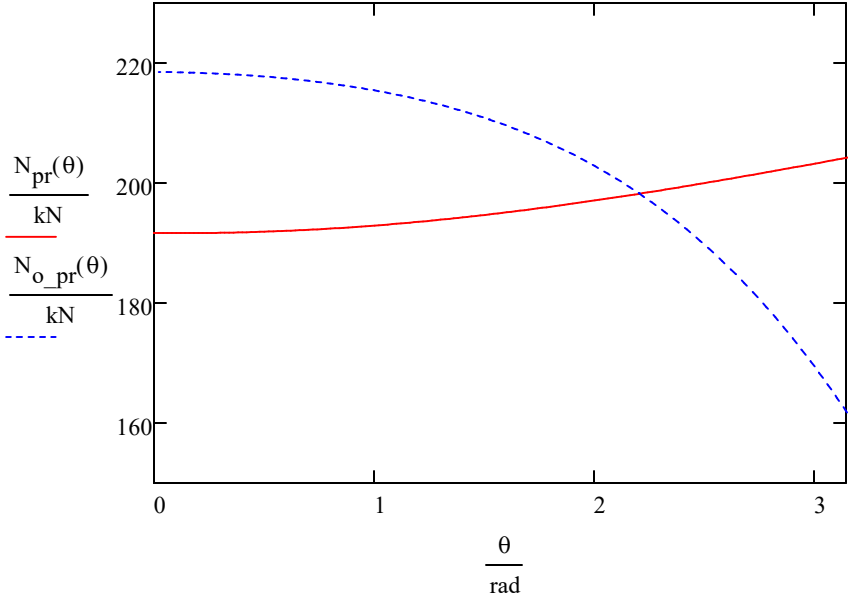
solve equation for 1 $N_{o_pr}(\theta) := \text{root}(f_o(N_{o_pr}, \theta) - 1, N_{o_pr}, 10\text{kN}, 300\text{kN})$

small crack size $N_{o_pr}(\theta_{88\%}) = 216.782 \cdot \text{kN}$

medium crack size $N_{o_pr}(\theta_{76.5\%}) = 211.118 \cdot \text{kN}$

large crack size $N_{pr}(\theta_{61.5\%}) = 199.485 \cdot \text{kN}$

Capacity Perry: Crack closes vs Crack opens



When crack is closing, we assume full bearing in the crack surface until failure. Only reduction in capacity is due to holes, as the crack increases the holes are getting closer to neutral axis. Hence, the increase in capacity with increase in crack size.

Based on the test result there is an estimated eccentricity in the test setup at about 1.5-2 mm, For the cases where the crack is opening the crack is facing in a direction where the eccentricity due to the holes are working against the eccentricity in the rig. Hence, smaller total eccentricity. For the crack closing the specimens were placed with the crack facing the opposite direction thus the opposite effect. The total eccentricity becomes larger.

buckling Secant formula

Crack closes - considering reduced capacity onley due to holes

$$u(N_s, \theta) := \frac{N_s}{N_E} \cdot \left(1 + \frac{e_{\text{tot}}(\theta) \cdot r}{I_h(\theta)} \cdot A_{\text{hs}} \cdot \sec\left(\frac{\pi}{2} \cdot \sqrt{\frac{N_s}{N_E}}\right) \right) - \frac{N_d}{N_E}$$

$$N_s(\theta) := \text{root}(u(N_s, \theta), N_s, 1\text{kN}, 300\text{kN})$$

<i>small crack size</i>	$N_s(\theta_{88\%}) = 183.272 \cdot \text{kN}$
<i>medium crack size</i>	$N_s(\theta_{76.5\%}) = 186.486 \cdot \text{kN}$
<i>large crack size</i>	$N_s(\theta_{61.5\%}) = 192.913 \cdot \text{kN}$

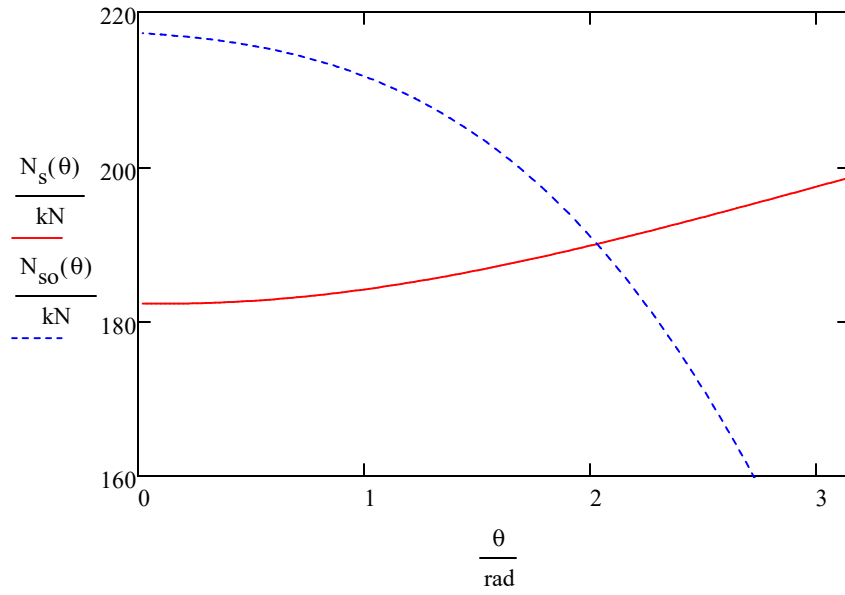
Crack opening - considering reduced momentcapacity due to crack

$$u_o(N_{\text{so}}, \theta) := \frac{N_{\text{so}}}{N_E} \cdot \left(1 + \frac{e_{o_tot}(\theta) \cdot y_{\text{max}}(\theta)}{I_c(\theta)} \cdot A_{\text{hs}} \cdot \sec\left(\frac{\pi}{2} \cdot \sqrt{\frac{N_{\text{so}}}{N_E}}\right) \right) - \frac{N_d}{N_E}$$

$$N_{\text{so}}(\theta) := \text{root}(u_o(N_{\text{so}}, \theta), N_{\text{so}}, 1\text{kN}, 300\text{kN})$$

<i>small crack size</i>	$N_s(\theta_{88\%}) = 183.272 \cdot \text{kN}$
<i>medium crack size</i>	$N_s(\theta_{76.5\%}) = 186.486 \cdot \text{kN}$
<i>large crack size</i>	$N_s(\theta_{61.5\%}) = 192.913 \cdot \text{kN}$

Capacity Secant: Crack closes vs Crack opens



Capacity: Perry Robertson and Secant

